UNIVERSITY OF OKLAHOMA

GRADUATE COLLEGE

AMPLITUDE-FREQUENCY TRADEOFFS IN THE ACTIVE SENSORY AND COMMUNICATION SIGNAL OF A WEAKLY ELECTRIC FISH

A THESIS

SUBMITTED TO THE GRADUATE FACULTY

in partial fulfillment of the requirements for the

Degree of

MASTER OF SCIENCE

By

ZHICONG CHU
Norman, Oklahoma
2017

AMPLITUDE-FREQUENCY TRADEOFFS IN THE ACTIVE SENSORY AND COMMUNICATION SIGNAL OF A WEAKLY ELECTRIC FISH

A THESIS APPROVED FOR THE
DEPARTMENT OF BIOLOGY

BY

_____
Dr. Michael Markham, Chair

_____
Dr. Rosemary Knapp

_____
Dr. Christian Lemon

Table of Contents

List of Tables

Chapter 1

Chapter 2

List of Figures

Chapter 1

Chapter 2

Chapter 3

Abstract

Animal communication signals play an important role in behavioral processes to ensure fitness and survivorship of individuals within a species. Weakly electric fish produce communication signals that could be among the most energetically expensive signals in the animal kingdom. These electric signals underlie an active sensory modality (electroreception) as well as a primary communication modality. The weakly electric fish *Eigenmannia virescens* generates constant, quasi-sinusoidal electric organ discharges (EODs) at a frequency of 200-600Hz. The EOD signals are produced by the summed action potentials of electrocytes - the electrically excitable cells of the electric organ (EO). Electric signals with stronger intensity bring adaptive advantages such as better resolution for electrolocation and higher efficacy of elctrocommunication, but also require larger energetic investments. Two signal features, EOD amplitude (EODa) and EOD frequency (EODf), are likely the primary determinants of the energetic costs of the EOD. Previous studies have verified the positive relationship between EODf and signal metabolic costs via both electrocyte model estimations at the cellular level and whole-animal respirometry measurements at the organismal level. Experimental evidence from behavioral studies of electric fish under energetic stress also suggest a correlation between EODa and signal energetic demands. I estimated and examined the combined roles of energetic limitations and sensory effectiveness on signal modulation in *E. virescens* via numerical simulations and behavioral experiments. Computational simulations of single electrocytes revealed a strong positive relationship between EODf and signaling costs, but no clear relationship between EODa and signaling costs. In subsequent behavioral experiments, I hypothesized that an increase in EODa or EODf

would be offset by a compensatory decrease in the other. However, I did not observe clear tradeoffs between EODa and EODf. Future studies of the relationship between EODa, EODf, and signal energetics are needed to more fully investigate the causes and mechanisms through which animals regulate their communication signals and balance the costs and benefits associated with signaling.

Chapter 1: Overview of Electric Sensory and Communication Signals

Costs and Benefits of Animal Communication Signals

Animal communication is an exchange of information between animals, especially individuals of the same species. It occurs when the actions or perceptual cues produced by one animal affect another animal. Usually the signal's sender, receiver, or both obtain some benefit from the interaction. For instance, gibbons make vigorous vocal calls to advertise territory and warn their competitors (Klause, 2001), juvenile herring gulls peck at the red spots on the beaks of their parents as a signal of hunger (Tinbergen and Perdeck, 1950), and honey bees perform waggle dances in the hive after foraging to share information about the direction and distance to food and water sources (Kirchner, 1993). Natural selection generally favors signals that maximize signal intensity relative to background noise (Endler, 1992). Signal generation, along with transmission degradation and receptor characteristics, together determine the quality of the received signal. As a result, selective pressures generally favor signals with higher intensity (Endler, 1992). For example, bird chicks with louder begging calls tend to receive more food from their parents and thereby outcompete their nest mates (Leech and Leonard, 1997). Secondly, the evolution of signal transmission has driven signals in the direction of less distortion and attenuation. For example, males of some animal species produce signals that transmit effectively only during particular seasons. Males that transmit signals during these specific time periods obtain more mating opportunities than males that transmit signals during other periods (Endler, 1992). Finally, signal receptor mechanisms have evolved in ways that increase information efficiency and signal reliability. The presence of unintended signals or background

noise facilitated the evolution of signal receptors that minimize interference and filter out noise (Endler, 1993).

In contrast to the many benefits of communication signals are the costs of these signals, which include opportunity cost, predation risk, and metabolic cost. Opportunity costs arise when an animal must choose between two mutually exclusive behaviors. Exhibiting one behavior precludes the potential benefit of the alternative behavior. For example, when an animal produces signals to attract a mate, it loses that period of time for foraging (Bradbury and Vehrencamp, 1998). Predation risks caused by communication signals are also widespread in the animal world. The signals of courtship, for example, can alert nearby predators and make the sender vulnerable. Finally, communication signals incur metabolic costs because they require energetic investment for production of the signal.

The energetic costs of communication signals vary widely among different species. According to a comparative study of different taxa and animal groups (Stoddard and Salazar, 2010)(Figure 1), orthopteran species spend the highest amount of energy on signaling. Wolf spiders, orthoptera, and frogs have the highest ratios of energy devoted to signaling to energy spent at rest (Stoddard and Salazar, 2010). However, after taking the daily duration of signaling into consideration, the corrected energetic costs (Table 1) for some weakly electric fish species with only moderate moment-to-moment signal costs ultimately are among the highest on a 24-hour basis because these electric signals are emitted constantly (Markham et al., 2016). Generally, animals whose communication systems are coupled with an active sensory modality require higher metabolic costs for signaling. The self-generated energy of active sensing

allows better control on signal characteristics but usually has higher energetic demands on the sensory system as a tradeoff (Nelson and MacIver, 2006).

Electric Communication and Sensory Systems of Weakly Electric Fish

Weakly electric fish use self-generated electric signals to image their environment as well as communicate with each other. These fish generate electric fields around their bodies through the electric organ discharge (EOD) produced by a specialized electric organ (EO). The EO is composed of electrocytes - highly electrically excitable cells responsible for producing electric signals. With electroreceptors on the skin surface, weakly electric fish detect distortions of the electric field. After neural processing and analysis of these distortions, the sensory system can characterize surrounding objects as prey items or obstacles. The resolution of the sensory image is affected by many factors including signal amplitude, water conductivity, and the sampling rate, which is determined by EOD frequency (Hopkins, 1999). The electric sensory signals generated by weakly electric fish enable them to navigate and communicate with conspecifics even in absolute darkness and highly turbid waters where vision is ineffective.

Within the broad category of weakly electric fish, the African Mormiridae and the South American Gymnotiformes evolved independently (reviewed in Markham, 2013). Electric signal waveforms are highly diverse and distinct to different species. However, these signals can be broadly categorized as pulse-type or wave-type based on their EOD rates. Pulse-type fish produce EODs with very low rates and long irregular intervals while wave-type fish generate continuous signals with regular discharges at high frequencies (Bennett, 1970; Stoddard, 2009). The wave-type fish produce signals

over a wide range of frequencies, from 30 Hz to 2,200 Hz (Albert and Crampton, 2005). High-frequency EODs enable faster sampling by the sensory system with more information, leading to enhanced detection of rapid changes in the environment. In addition, high-frequency signals shift the peak energy of the signal towards higher frequency bands, which reduces the risk of being detected by electroreceptive predators that detect only low-frequency components in the range of 0 to 100 Hz (Stoddard and Markham, 2008).

Energetic Costs of EOD Production

Although signals with high frequency and large intensity bring adaptive benefits to weakly electric fish, the energetic cost of these signals likely constrains signal generation. This conclusion has been recently supported by both experimental and theoretical analyses. Two studies that independently estimated the metabolic costs of EOD production via theoretical approaches revealed that signaling occupied 10-30% of the daily energy budget in weakly electric fish (Markham et al., 2013; Salazar et al., 2013). Experimental evidence also suggests that EOD production can take up approximately 22% of the daily energy budget in pulse-type fish (Salazar and Stoddard, 2008) and 30% of the daily energy budget in wave-type fish (Lewis et al., 2014).

The EOD is the summation of simultaneous or near-simultaneous action potentials (APs) produced by more than a thousand electrocytes. Ultimately, the energetic cost of EOD production likely arises predominantly from the metabolic cost of the electrocyte action potentials (APs). The electrocyte AP is typical of any excitable cell, characterized by depolarization and repolarization of the electrocyte membrane when Na^+ ions flux into the cell through voltage-gated Na^+ channels and K^+ ions flux

out of the cell through voltage-gated K^+ channels. The movement of these ions is driven by their concentration gradients across the electrocyte membrane. The energy consumption of the AP is primarily driven by the Na, K-ATPase, which must hydrolyze ATP to restore the ionic gradients across the membrane after each AP (Bean, 2007).

Consequences of EOD Metabolic Costs

Because of the high energetic costs of the EOD, some weakly electric fish species exhibit circadian rhythms of EOD production to conserve energy. The day-night oscillation of EOD duration, amplitude, and rate have been intensively studied. In general, weakly electric fish are less active and maintain a relatively low EODa during the day. EODa begins to increase in the late afternoon and the fish become active by sunset. Around an hour after the beginning of darkness, EOD waveforms are then fully enhanced with even higher signal amplitudes (Stoddard et al., 2005). Through the circadian rhythms of EOD signals, weakly electric fish can regulate their metabolic demands and conserve energy for the night time hours when they are active.

Weakly electric fish also modulate their signal amplitude in response to metabolic stress. During energetic constraints when signals of large intensity become unaffordable, decreasing EODa could be an effective way of reducing metabolic costs. Experimental evidence from recent behavioral studies supports this speculation. Under hypoxia, the wave-type fish *Eigenmannia virescens* reduces EODa as a response to this acute energetic constraint (Reardon et al., 2011). Similarly, during food deprivation, which is recognized as mild metabolic stress, *E. virescens* also decrease EODa drastically compared with periods of normal feeding (Sinnett and Markham, 2015).

In this study, I explored the cost-benefit balance in the electric signals of the high-frequency wave-type species *E. virescens*. The benefits of high amplitude and high frequency EODs are better electrolocation performance and higher communication efficiency. On the other hand, signals with both higher frequency and amplitude require larger energy investment. This cost-benefit balance raises the issue of a potential tradeoff between signal amplitude and frequency. Specifically, the research question I addressed in this study is whether an increase in one parameter is offset by a decrease in the other.

Tables

Table 1: Metabolic costs of animal communication signals from experimental measurements (adapted from Markham et al., 2016).

Organism	Source	Signal ATP $g^{-1}s^{-1}$	Duration (hours d^{-1})	24-h ATP_{Signal}/ATP_{Rest}
Arachnids				
Wolf Spider *Hogna rubrofasciata*	Kotiaho et al. (1998)	$1.71 \sim 10^{17}$	2	1.73
Insects				
Trilling cricket *Anurogryllus arboreus*	Prestwich and Walker (1981)	$1.36 \sim 10^{17}$	2	0.95
Short-tailed cricket *A. muticus*	Lee and Loher (1993)	$3.38 \sim 10^{17}$	2	0.44
Trilling Katydid *Euconocephalus nasutus*	Stevens and Josephson (1977)	$5.89 \sim 10^{17}$	2	0.50
Trilling cricket *Gryllotalpa australis*	Kavanagh (1987)	$1.82 \sim 10^{17}$	2	0.97
Amphibians				
Squirrel treefrog *Hyla squirella*	Prestwich et al. (1989)	$7.88 \sim 10^{16}$	2	1.26
Birds				
Carolina Wren *Thryothorus ludovicianus*	Eberhardt (1994)	$3.37 \sim 10^{17}$	2	0.21
Gymnotiform weakly electric fish				
Feathertail knife fish (female) *B. gauderio*	Salazar and Stoddard (2008)	$5.97 \sim 10^{14}$	24	0.04
Feathertail knife fish (male) *B. gauderio*	Salazar and Stoddard (2008)	$4.74 \sim 10^{15}$	24	0.13
Glass knife fish (200 Hz) *E. virescens*	Lewis et al. (2014)	$4.82 \sim 10^{14}$	24	1.29
Glass knife fish (300 Hz) *E. virescens*	Lewis et al. (2014)	$1.30 \sim 10^{15}$	24	2.29
Glass knife fish (500 Hz) *E. virescens*	Lewis et al. (2014)	$3.47 \sim 10^{15}$	24	3.13

Figures

Figure 1: Metabolic costs of signals relative to metabolic costs while at rest of different animal species, expressed as the natural logarithm of oxygen consumption. Horizontal lines represent the same signal cost. Diagonal lines represent the same proportion of energy budget spent on communication signals relative to resting metabolism. (Adapted from Stoddard and Salazar, 2010)

Figure 1

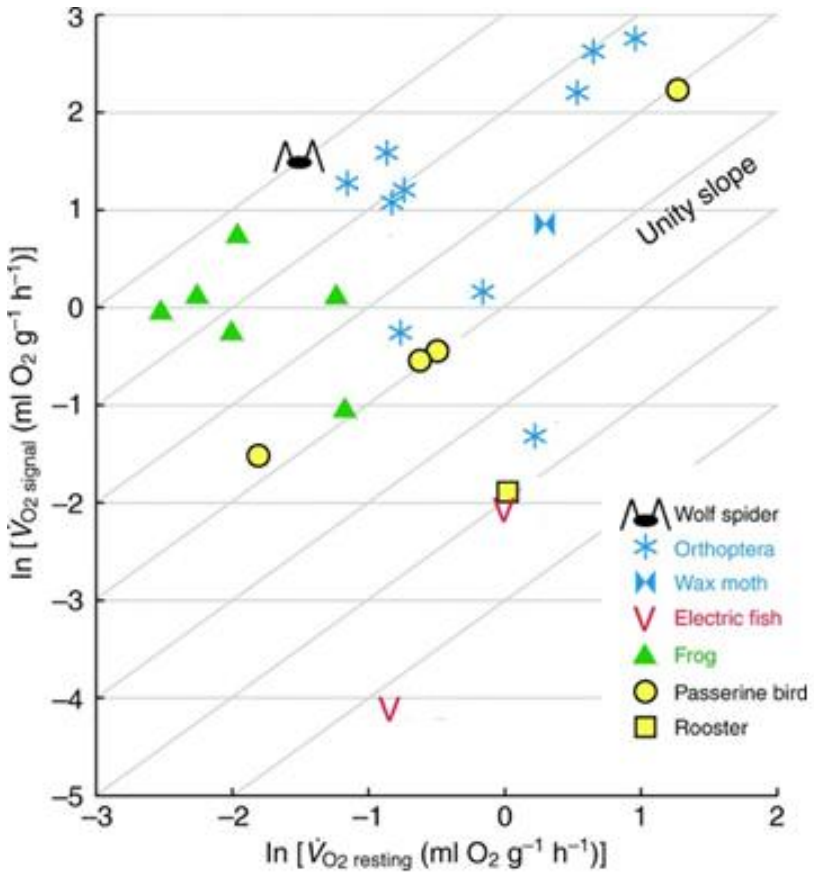

Chapter 2: Computational Simulations

Introduction

The metabolic cost of generating the multi-function electric organ discharge (EOD) in weakly electric fish comes primarily from the cost of generating simultaneous APs in ~1,000 electrocytes in the electric organ. Electrocyte APs are initiated by a medullary pacemaker nucleus that relays a spinal command via motorneurons that form cholinergic synapses on the electrocytes. As in any excitable cell, electrocyte APs begin with a depolarization phase driven by Na^+ flux into the electrocyte through voltage-gated Na^+ channels. As a result of this depolarization, membrane potential increases, causing voltage-gated K^+ channels to open. Consequently, the concentration gradient of K^+ across the membrane leads to efflux of K^+ and a decrease in membrane potential, which characterizes the repolarization phase of the AP. After each AP, ATP-driven ATPases pump Na^+ out of the cell and pump K^+ in to the cell to restore the ion gradients necessary for AP production. In each cycle of Na,K ATPAse activity, one ATP is hydrolyzed to move three Na^+ to the extracellular space and bring two K^+ into the intracellular space. This process accounts for the vast majority of the energetic cost associated with the AP, and presumably the majority of the metabolic costs of EOD production. Therefore, estimates of energetic demand of firing APs are typically based on the measurement of the total Na^+ current, which drives the activity of these Na^+/ K^+ ATP pumps.

E. virescens is a wave-type electric fish that produces a regular and continuous electric sensory and communication signal. Their electrocytes can generate EODs at high frequencies of 200-600 Hz (Scheich, 1977), making the signal extremely

expensive energetically (Lewis et al., 2014). Additionally, *E. virescens* is one of the most intensively studied electric fish species, with extensive data available from behavioral, endocrine, and physiological studies, making them a good model for investigating the energetics of EOD signals. The electric signals produced by these fish account for a large portion of their daily energetic budget (Lewis et al., 2014). Na^+ influx during the AP in a single electrocyte can be extremely high, estimated to be ~3–9 × 10^{10} Na^+ during each AP based on recent numerical simulations (Markham et al., 2013) and directly measured with electrophysiological methods to be 6.6 × 10^{10} Na^+ per AP, thereby requiring 2.2 × 10^{10} ATP per AP (Lewis et al., 2014). The energetic cost of an AP in *E. virescens* electrocytes is two orders of magnitude greater than in mammalian neurons (Attwell and Laughlin, 2001; Howarth et al., 2012; Lewis et al., 2014).

Unlike other closely-related electric fish species where the AP is terminated by voltage-gated K^+ channels, the AP in *E. virescens* electrocytes is terminated by Na^+-activated K^+ (K_{Na}) channels. An early computational model suggested that these K_{Na} channels make the *E. virescens* electrocyte 30% more energy efficient than cells with classic voltage-gated K^+ (Kv) channels (Markham et al., 2013). However, recent experimental work (Ban et al., 2015) and computational simulations (Ban et al., 2015, Joos et al., 2016) cast doubt on this conclusion.

In weakly electric fish species, metabolic costs of EOD generation can be affected by various factors including EOD waveform, EODf, and EODa. Energetic costs increase when EODf increases (Lewis et al., 2014) and it is reasonable to predict that energetic costs also increase when EODa increases. In some species, including *E.*

virescens, EODa can change by as much as 50% on a circadian rhythm and in response to social encounters (Markham et al., 2009; Sinnett and Markham, 2015). In both pulse-type and wave-type fish, EODf can change transiently in response to social conditions or novel environmental events (Moller, 1970; Moller and Richard, 1973; Zakon et al., 2002). The best understood case is the jamming avoidance response (JAR).

The JAR is a naturally occurring social behavior of weakly electric fish that has been intensively studied (Heiligenberg, 1973; Zakon et al., 2002; Carlson and Kawasaki, 2007). Wave-type fish that perform the JAR emit steady quasi-sinusoidal EODs. For instance, fish in the genus *Eigenmannia* generate electric signals ranging from 200 to 600 Hz with a frequency variation that less than 0.3% over a 10-min span (Bullock et al., 1972). If a neighboring conspecific discharges at a similar frequency to the fish's EODf, their sensory signals will be jammed (by destructive interference), leading to degradation of sensory effectiveness. As a result, when two fish with similar signal frequencies are in proximity, the destructive interference between the two EOD waveforms introduces sensory confusion (Heiligenberg, 1973). As a response, the fish with higher frequency further increases its EODf while the fish with lower frequency decreases its frequency so that the signals shift away from each other and avoid interference. The frequency change associated with the JAR can provide insights to questions related to energetics and social communication in these fish (Bullock et al., 1971).

Here, I investigated the potential frequency-amplitude tradeoff in EOD signals of weakly electric fish. Specifically, will a change one of these features be accompanied by a compensatory change in the other? I used a computational model of the *E.*

virescens electrocyte (Ban et al., 2015) to study the dynamics of changing electrocyte AP amplitude and frequency and then estimate the corresponding changes in energy consumption. I hypothesized that both signal features, amplitude and frequency have positive effects on energetic demand during EOD generation. I predicted positive correlations between the two signal features and estimated ATP expenditure in the biophysical model of a single electrocyte in *E. virescens.* The alternative hypothesis was that either one of the two signal features, amplitude or frequency had no effect or negative effect on energetic costs of EOD production.

I also investigated the energetic consequences of EODf changes associated with the JAR. Because the JAR can be easily reproduced and quantified in experimental settings, numerical simulations of JARs in this study should provide predictions that can be tested experimentally *in vivo*. The model estimates from the present study could additionally provide novel insights on the signaling behaviors of weakly electric fish.

Methods

Computational simulation of the electrocyte

Based on a biophysical model described previously (Ban et al., 2015), I simulated a single *E. virescens* electrocyte with a modified three-compartment model including an active anterior compartment, a passive central compartment and an active posterior compartment. The Hodgkin-Huxley formalism was used to simulate changes in electrocyte membrane potentials and ionic currents across the membrane. I applied simulated cholinergic synaptic currents only to the posterior compartment. I also simplified the Na^+ entry, diffusion and pumping in the model to dynamically simulate

changes of Na^+ concentration in the three compartments. From confocal 3D reconstructions of electrocytes in *E. virescens* (Ban et al., 2015), I obtained surface area values of the posterior and anterior regions of 0.35 mm^2 and 0.2 mm^2, respectively. Based on these surface area values, the capacitance for the posterior compartment was set to 48.0 nF and the capacitance of the anterior compartment was set to 18.0 nF. The central compartment was approximated as a cylinder with the dimensions of 0.95 mm in length and 0.6 mm in diameter (Ban et al., 2015). Thus, the capacitance of the central compartment was estimated to be 18 nF, based on this approximation. All equations were coded in Matlab (Mathworks, Inc. Natick MA). Differential equations were integrated via Euler's method with time steps of 5×10^{-8} sec. Model parameters are shown in Table 1.

The passive central compartment was coupled to the active posterior and anterior compartments. The current exchange and dynamic coupling was represented by the current balance equation that includes only passive leak (I_L) fixed at 5 μS:

$$C_m \frac{dV_c}{dt} = -I_{Lc} + g_w(V_a - V_c) + g_w(V_p - V_c) \qquad (1)$$

where V_a, V_c, and V_p represent the membrane voltage of the anterior, central, and posterior compartments, respectively, and g_w represents the coupling conductance between compartments, fixed at 322 μS.

The current balance equations for the active posterior and anterior compartments were formulized respectively as:

$$C_m \frac{\mathrm{dV_p}}{\mathrm{dt}} = I_{Syn}(t) - \mathrm{I_{Na}} - \mathrm{I_{Lp}} + g_w(V_c - V_p) \qquad (2)$$

$$C_m \frac{\mathrm{dV_a}}{\mathrm{dt}} = -\mathrm{I_{KNa}} - \mathrm{I_R} - \mathrm{I_{La}} + g_w(V_c - V_a) \qquad (3)$$

where I_{Syn} is synaptic current, I_{Na} represents Na^+ current, I_{KNa} represents the Na^+-activated K^+ current, and I_R represents the inward rectifier K^+ current. I_L is the leak current, whose value was given for all the three compartments by Equation 4:

$$I_L = \bar{g}_{\mathrm{L}}(\mathrm{V} + 95) \qquad (4)$$

where $\bar{g}_{\mathrm{L}}$ represents the maximum conductance of the leak channel.

The synaptic current, I_{Syn}, applied to the posterior compartment, was given by Equation 5:

$$I_{Syn} = \bar{g}_{Syn}\, g_{Syn(t)}(V_p - 15) \qquad (5)$$

with the time series of 10 alpha waveforms denoted by $g_{Syn(t)}$ and generated from the discrete time equation:

$$g_{Syn(n+2)} = 2\left(1 - \frac{T}{\tau}\right) g_{Syn(n+1)} - \left(1 - \frac{T}{\tau}\right)^2 g_{Syn(n)} + \left(\frac{T}{\tau}\right)^2 x(n)$$

(Graham and Redman, 1993), where *T* represents the integration of time step and τ represents the time constant. The onset time of the synaptic inputs was specified via the binary series *x(n)* and the resulting time-series $g_{Syn(n)}$ was normalized to make $0 \leq g_{Syn(n)} \leq 1$.

The Na^+ current I_{Na} was formulized as the sum of a transient component (I_{NaT}) and a persistent component (I_{NaP}), and their values are given in Equations 7 and 8:

$$I_{NaT} = \bar{g}_{Na} m^3 (1 - \gamma) h (V_p - E_{Na}) \qquad (7)$$

$$I_{NaP} = \bar{g}_{Na} m^3 \gamma (V_p - E_{Na}) \quad (8)$$

where $0 < \gamma < 1$. Based on the Nernst equation $E_{Na} = 25.7ln(114/[Na_P])$, the Na^+ equilibrium potential E_{Na}, was allowed to change and was determined by Na^+ concentrations in the posterior compartment (Na_P). I assumed a fixed extracellular Na^+ concentration at 114 mM and temperature of 25 °C.

The K^+ currents of the anterior compartment were given by equations 9 and 10:

$$I_{KNa} = \bar{g}_{KNa} n^4 s^4 (V_a + 95) \quad (9)$$

$$I_R = \bar{g}_R \left(\frac{1}{1+\exp(\eta_R(Vm+110))} \right) (V_a + 95) \quad (10)$$

The gating variables of ion channels denoted as *m*, *n*, and *h* in Equations 7-9 were given by Equations 11-13:

$$\frac{dj}{dt} = \alpha_j (1 - j) - \beta_j (j) \quad (11)$$

$$\alpha_{\mathrm{j}} = k_{\alpha \mathrm{j}} \exp(\eta_{\alpha \mathrm{j}} \mathrm{V}) \quad (12)$$

$$\beta_{\mathrm{j}} = k_{\beta \mathrm{j}} \exp(\eta_{\beta \mathrm{j}} \mathrm{V}) \quad (13)$$

where *j* = *m*, *n*, or *h*.

I simulated the Na^+-dependence of the K_{Na} channel and I_{KNa} with another gating variable, s. The gating variable s was given by Equation 14:

$$\frac{ds}{dt} = k_{\mathrm{f}} [Na_A] (1 - \mathrm{s}) - k_{\mathrm{b}} \mathrm{s} \quad (14)$$

where Na_A represents Na^+ in the bulk cytoplasm in the anterior compartment.

The Na^+ concentration in each compartment was modeled based on volumes of the three compartments. According to the estimates from 3D reconstructions of electrocytes (Ban et al., 2015), the volumes of posterior and anterior compartments were, respectively, 4.2×10^7 μm^3 and 1.7×10^7 μm^3. The central compartment was approximated as a cylinder of 0.95 mm in length and 0.6 mm in diameter, giving a volume of 2.7×10^8 μm^3. The initial Na^+ concentration in all three compartments was set to 15 mM. The dynamics of Na^+ concentration in the posterior compartment was given by Equation 15:

$$\frac{d[Na_P]}{dt} = p + \frac{q}{Vol_P} - \delta([Na_P] - [Na_C])\frac{\lambda_P}{\lambda_C} - b_P[Na_P] \qquad (15)$$

where p is the Na^+ leak and q represents the number of Na^+ in moles binding with the cholinergic receptors and entering Na^+ channels. The equation for q was:

$$q = \frac{dt(2\,I_{Syn} + I_{Na})10^{-12}}{eL} \qquad (16)$$

where $dt(2I_{Syn} + I_{Na})$ represents the integrated Na^+ current in nA*ms. The value of $dt(2I_{Syn} + I_{Na})$ was then multiplied by 10^{-12} to yield electric charge in Coulombs, and then divided by the elementary charge on a monovalent cation, e, to yield the number of Na^+ ions from Na^+ current, further divided by Avogadro's constant, L, to yield the quantity of Na^+ ions in moles. Synaptic current I_{Syn} was multiplied by 2 to account for Na^+ entry from synaptic input I_{Syn}. The maximum synaptic conductance g_{Syn} arises from cholinergic receptors and I assumed that the permeability of Na^+ is twice that of K^+.

Diffusion rate of Na^+ between compartments was determined by δ (the diffusion rate constant), Na^+ concentration gradients between compartments and the ratio of the

volumes between compartments (λ). Na^+ reset was modeled by the fractional pumping rate b_P that represents how quickly Na^+ is pumped out to the extracellular space from the posterior compartment.

Na^+ concentration in the central compartment, affected only by diffusion to and from the other compartments, was given by Equation 17:

$$\frac{d[Na_C]}{dt} = \delta([Na_P] - [Na_C])\frac{\lambda_P}{\lambda_C} - \delta([Na_C] - [Na_A])\frac{\lambda_C}{\lambda_A} \quad (17)$$

Na^+ concentration in the posterior compartment was given by Equation 18. Factors affecting the posterior compartment Na^+ concentration include diffusion into and out of the central compartment, and the fractional pumping rate b_A that specifies how quickly Na^+ is pumped out into the extracellular space from the anterior compartment.

$$\frac{d[Na_P]}{dt} = \delta([Na_C] - [Na_A])\frac{\lambda_C}{\lambda_A} - b_A[Na_A] \quad (18)$$

Model simulations across parameter space

Forty thousand different parameter combinations were selected as the model inputs by random generation from predetermined ranges of stimulus frequency and the following ionic conductances: $\bar{g}_{Na}$, $\bar{g}_{KNa}$, $\bar{g}_R$, $\bar{g}_{\mathrm{La}}$, $\bar{g}_{\mathrm{Lp}}$, and $\bar{g}_{Syn}$ (Table 1). With these inputs, the biophysical model of the single electrocyte was able to output ionic current time series and EOD waveforms associated with every combination of input variables. EODa and frequency were then computed from the waveforms generated and set as the predictor variables of the prediction model. ATP consumption was also estimated from the total Na^+ currents and defined as the response variable of the prediction model.

Multiple filters were established to rule out abnormal data, including simulations with non-typical EOD waveforms whose voltage potentials never fell back below the threshold, incorrect firing frequencies that deviated too much (frequency difference > 6 Hz) from stimulus frequencies and inappropriately low ratios (< 0.3) between the inward posterior current and the outward anterior current.

Data interpolation

I used the Delaunay triangulation approach (Amidror, 2002) to perform data interpolation on 3-dimensional scatter plots of two input variables, voltage amplitude and signal frequency, and one response variable, estimated ATP consumption per millisecond. I applied natural-neighbor interpolation to the scattered data sets to reconstruct both a continuous surface as well as a function that extended and covered sample points within the predetermined parameter space. Interpolation and relevant predictions were coded in Matlab (Mathworks, Inc., Natick, MA).

Grid approximation for optimal energetic strategies

The model took ionic conductance inputs within the physiologically relevant ranges shown in Table 1. With these different combinations of ionic conductances, the biophysical model was able to generate EOD signals of the same or similar signal amplitude and frequency, but with vastly different energetic costs. Based on the optimality model in ecology (Parker and Smith, 1990), I examined the features of model cells that achieved the highest energetic efficiency while obtaining electrocyte APs of different amplitude and frequency combinations. To approximate optimal energetic strategies, it was necessary to identify the model cell with the lowest energetic cost at

every combination of amplitude and frequency. To do this, I graphed the scattered data in the 3-dimensional space, with the inputs amplitude and frequency on the x and y axes and the response variable ATP per millisecond on the z axis. Then, I projected all sample points vertically to the xy plane (Figure 2A). Within the parameter space of x and y, I created a grid with grid intervals that covered the full range of amplitudes and frequencies. The grid intervals were subdivided to achieve pre-specified column width and row height values (Fig. 2B). For every projected sample point, its Euclidean distances to all grid points were computed. Based on the minimum Euclidean distances, the x and y coordinates of each projected sample point were set to the closest grid point (Fig. 2B,C). After these adjustments to the x-y coordinates, there were model cells with varying energetic costs at each grid point (Fig. 2C). The model cell with the lowest energetic cost at each grid point was selected then traced back to its original data point in the 3D space. This resulting subset of model cells, the Cells of Optimized Energetics (COEs) were selected as data points for subsequent analysis and all the other model cells were excluded (Fig. 2D). This data interpolation approach was then applied to reconstruct the continuous surface and function that cover the COE model cells (Fig. 2D).

JAR simulation

To simulate the JAR in the set of COEs, I further assumed that *E. virescens* electrocytes are not able to change their ionic conductances upon shifting EODf. In order to determine how JAR-related frequency changes affect energetic efficiency, I started with the full set of COEs and reran the computational models with the same ionic conductances but drove the cells at frequencies +5 Hz, +10 Hz, -5 Hz, and -10 Hz from

their baseline frequencies to simulate both an upward and downward JAR. The estimated ATP consumption of each model cell after this frequency shift was then compared to the energetic costs of the COE for the new amplitude and frequency. The difference of energetic costs between the frequency-shifted COE and the resident COE was denoted as ΔATP, the difference in ATP consumption between a cell optimized for a particular amplitude and frequency versus the ATP consumption of a COE cell shifted to that amplitude and frequency.

Results

Effects of AP amplitude and frequency on energetic costs

Within the entire set of model cells consisting of 40,000 combinations of ionic conductances, 81.37% (32,548) of the model cells passed the filters and generated normal AP waveforms at the appropriate frequency. The peak-to-peak voltage amplitude across the electroycte's anterior membrane was defined as the signal amplitude and was measured from the AP waveform. Energetic costs of producing the signal (number of ATP per millisecond and number of ATP per AP) were computed from integrated Na^+ current in the model output. The biophysical model estimated an energetic cost of ~ 1-4 × 10^{10} ATP molecules per millisecond and ~5-8 × 10^{10} ATP molecules per AP, which was comparable with but slightly higher than previous measurements of ~2 × 10^{10} ATP molecules per AP (Lewis et al, 2014). The 3-dimensional scatterplot of amplitude, frequency and energetic costs (Fig. 1) displays a surface with considerable variation in the z-axis (ATP/ms) because the plot includes cells with all combinations of ion conductances and stimulus frequencies that

successfully generated normal AP waveforms at each combination of amplitude and frequency.

The subset of COE cells consisted of 2.22% of the total functional model cells (721 out of 32,548) (Fig. 2D). The data interpolation method for selecting this subset of COE cells was successfully validated by comparing grids of different resolutions (Appendix A). The reconstructed surface of COE cells showed strong positive correlation between firing frequency and ATP consumption. There are two patterns apparent for amplitude. For COE cells with a frequency lower than ~400 Hz, a subtle negative effect of amplitude is apparent in estimated energetic costs. In contrast, for COE cells with frequencies greater than 400 Hz, there is a slightly positive correlation between amplitude and estimated energetic costs, especially at high amplitudes. Marginal effects of amplitude and frequency on the number of ATP per unit time were checked via simple linear regression (Fig. 3), using the data points in the subset of optimal energetic strategies. Overall, a negative effect of signal amplitude was detected on ATP consumption (ATP per ms = $-1.129*10^{9}$ * Amplitude + $1.403*10^{11}$, $R^2= 0.407$, $p < 2.2*10^{-16}$). A positive effect of signal frequency was also observed on ATP consumption (ATP per ms = $9.706*10^{7}$* Frequency + $5.755*10^{7}$, $R^2= 0.881$, $p < 2.2*10^{-16}$).

Effects of simulated JARs

Simulated JARs within the set of COE model cells showed that, for either a positive or negative frequency change, the estimated metabolic costs for cells after the frequency change were almost universally higher than the resident cell at each

amplitude/frequency combination (Fig. 4). Overall, data points indicating positive ΔATP values (100% and 97.24% in +5 Hz and -5 Hz stimulus data sets, 95.96% and 96.86% in +10 Hz and -10 Hz stimulus data sets) far outnumbered data points with negative ΔATP values (Fig.4A,C,E,G). ΔATP increased as the baseline frequency increased, yielding a positive correlation in data sets of +5 Hz and -5 Hz frequency shifts ($\Delta ATP = 9.4198*10^{6} * Frequency - 8.0352*10^{8}$, $R^2 = 0.233$, $p = 7.71e-35$ for +5 Hz data set, $\Delta ATP = 1.3424*10^{7} * Frequency - 2.0679*10^{9}$, $R^2 = 0.323$, $p = 8.22*10^{-51}$ for -5 Hz data set) (Fig. 4B,D). ΔATP from a 10-Hz shift revealed very similar patterns of positive correlation between baseline frequency and ATP expenditure ($\Delta ATP = 1.1841*10^{7} * Frequency - 1.5518*10^{9}$, $R^2 = 0.225$, $p = 3.36*10^{-33}$ for +10 Hz data set, $\Delta ATP = 1.1869*10^{7} * Frequency - 1.5124*10^{9}$, $R^2 = 0.257$, $p = 9.53*10^{-39}$ for -10 Hz data set) (Fig. 4F,H).

Discussion

Target outputs can be achieved with a variety of conductance combinations.

One striking outcome of this study is that any given combination of electrocyte AP amplitude and frequency could be achieved by numerous model cells with vastly different complements of ionic conductances. This finding is consistent with a growing body of evidence that excitable cells can achieve particular action potential waveforms and patterns with highly varied combinations and densities of ionic conductances (reviewed by Marder and Goaillard, 2006). In the present results, the functional model cells at each frequency/amplitude combination exhibited a broad range of energetic efficiencies, raising the possibility that the particular combination of ionic conductances

expressed to achieve a target frequency and amplitude might be tuned to optimize the electrocyte's energetic efficiency, as is the case in other classes of excitable cells (Carter and Bean, 2009).

Effects of frequency and amplitude on energetic cost estimates

Based on the results from the present model, raising EODf caused dramatically higher energetic costs, while EODa had only a minor negative effect on ATP consumption of the model cells. This finding partially supported my hypothesis that both signal frequency and amplitude have positive effects on the energetic costs of generating the electric signal. However, the effect of amplitude on energetic demands in the present results was not as I hypothesized.

The effect of frequency on energetic costs of the electrocyte was strong and positive, based on the analysis of the COE cells. Surprisingly, within this subset of cells, energetic costs were not positively correlated with AP amplitude. Within the COE cells, the marginal effect of amplitude revealed slightly lower metabolic costs at higher signal amplitude, which seems counterintuitive. However, the three-dimensional reconstructed surface showed two different patterns of signal amplitude on estimated ATP consumption. At low frequency that was less than about 400 Hz, higher amplitude was correlated with lower energetic costs while at high frequency that was greater than 400 Hz, raising amplitude cost slightly more ATP within a fixed period of time. Based on the results of the current model, frequency appears to be more important than amplitude in determining the energetic costs of producing EOD signals, suggesting that changes in EODf would have greater impacts on signal energetics than changes in EODa.

This outcome stands in contrast to experimental studies where *E. virescens* were subjected to metabolic stress. During moderate metabolic stress caused by food deprivation, *E. virescens* responded by decreasing EODa, with little to no change in EODf (Sinnett and Markham, 2015). A similar outcome was observed during acute metabolic stress caused by hypoxia, where *E. virescens* respond by reducing EODa rather than EODf (Reardon et al., 2011).

The present results suggest that decreasing EODf is a much more effective strategy for reducing metabolic costs during metabolic stress. This modification not only would reduce expenditures associated with electrocyte Aps, but also the full cost of EOD production, which also includes synaptic costs, the costs of pacemaker function, and the costs of sensory circuits where thousands of cells fire 1:1 with the EOD (Krahe and Maler, 2014). An important remaining question, then, is why fish respond to metabolic stress by reductions in signal amplitude rather than reductions in EODf.

The metabolic effects of changing EOD frequency

Perhaps the strongest prediction to arise from the present study concerns the effects of transient changes in EODf associated with the JAR. When COE cell firing frequency was increased or decreased, this change produced a decrease in energy efficiency for more than 95% of the COE cells (assuming no change in ionic conductances). This effect was magnified in cells at higher frequencies, meaning that fish with higher baseline frequencies sacrifice more energetic efficiency during the JAR than fish at lower baseline frequencies. This outcome is consistent with recent experimental findings that increases in EODf are exponentially more expensive for fish

with higher baseline frequencies (Lewis et al., 2014). The present computational results lead to an additional prediction that the extent of frequency changes during the JAR should be smaller for fish with higher baseline frequencies.

In conclusion, the present modeling studies suggest a strong positive effect of EODf on energetic costs, but no clear effect of signal amplitude was observed. The effects of frequency in the current model are consistent with experimental observations that the metabolic cost of EOD production increases exponentially with frequency (Lewis et al., 2014), but are inconsistent with experimental findings that fish respond to metabolic stress with reductions in amplitude but not frequency (Reardon et al., 2011; Sinnett and Markham, 2015). Additional experimental investigation and theoretical/computational studies are needed to resolve these inconsistencies. With respect to the current computational efforts, it is entirely possible that the present model of the *E. virescens* electrocyte is incomplete in one or more important ways. One notable simplification is that the model treats the electrocyte as a three-compartment cell, which is potentially a gross oversimplification of the cell's highly complex morphology (Ban et al., 2015). Additionally the biophysical properties of the entire suite of ion channels expressed in electrocytes have not been fully characterized, so the present model is informed by incomplete experimental support. These shortcomings can be addressed through additional experimental work on the electrophysiology of electrocytes, as well as the development of computational models with higher spatial resolution and more precisely specified functional components.

Another consideration is that there could be other important features of the signal beyond peak-to-peak voltage amplitude and frequency that can influence signal

energetics. In electric engineering, voltage measurement integration is widely used to compute the power and energy of an electric signal, especially alternating current (AC) signals (Equation 19):

$$Es = \int_{-\infty}^{+\infty} |x(t)|^2 dt \qquad (19)$$

where Es represents the signal energy and $x(t)$ denotes the voltage measurement of the signal at time point t. Thus, for signals with the same frequency, peak-to-peak voltage amplitude by itself might not be sufficient to explain the effect of the signal on energetic costs. Future computational studies might benefit by considering other features of the signal waveform.

Tables

Table 1. Parameter values for the electrocyte model

Posterior Compartment		**Anterior Compartment**	
Parameter	**Value**	**Parameter**	**Value**
g_L	20 - 100 μS	g_L	60 – 180 μS
$\bar{g}_{Syn}$	300 - 600 μS	$\bar{g}_{KNa}$	6000 – 10,000 μS
$\bar{g}_{Na}$	800 – 1,600 μS	$\bar{g}_R$	100 - 400 μS
τ	0.07 ms		
γ	0.05		
k_{am}	13.6 ms^{-1}	k_{an}	1.2 ms^{-1}
η_{am}	0.0037 mV^{-1}	η_{an}	0.0095 mV^{-1}
$k_{\beta m}$	0.6894 ms^{-1}	$k_{\beta n}$	0.4448 ms^{-1}
$\eta_{\beta m}$	-0.0763 mV^{-1}	$\eta_{\beta n}$	-0.0155 mV^{-1}
k_{ah}	0.00165 ms^{-1}	k_f	50 $mM^{-1} \cdot ms^{-1}$
η_{ah}	-0.1656 mV^{-1}	k_b	200 ms^{-1}
$k_{\beta h}$	1.493 ms^{-1}	η_R	0.22 mV^{-1}
$\eta_{\beta h}$	0.11 mV^{-1}		
p	5 mM ms^{-1}		
δ	0.0019 $mm^2\ s^{-1}$	δ	0.0019 $mm^2\ s^{-1}$
b_P	0.3 mM ms^{-1}	b_A	0.7 mM ms^{-1}

Figures

Figure 1: 3D visualization of the prediction model of amplitude and frequency on energetic costs. (A) 3D scatter plot showing the relationship between EODf, EODa, and ATP consumption (ATP per ms) of the complete dataset from the entire parameter space. (B) Reconstructed surface via interpolation that covered all data points of the scatter plot in (A).

Figure 2: Schematic illustration of the grid approximation procedures for identifying cells of optimal energetics. (A) Data points were projected from the 3D space to the 2D plane of EODa/EODf. (B) Grids were established on the EODa/EODf plane and Euclidean distances were computed between projected points and grid points to identify the nearest grid point to each projected data point. The amplitude and frequency coordinates of projected points were then set to their closest grid points. (C) The model cells producing the lowest ATP consumption values were selected at each grid point and the selected cell was traced back to the original sample points in the 3D parameter space as a cell of optimized energetics (COE). Cells not selected as COE were excluded from subsequent analyses. (D) Surface interpolation on sample points of COEs and reconstruction of an approximated surface that covers all those data points.

Figure 3: Marginal effects of EODa and EODf on energetic costs in COEs. (A) Simple linear regression of EODa on ATP per ms in COEs. (B) Simple linear regression of EODf on ATP per ms in COEs.

Figure 4: 3D visualization and heat maps of ΔATP from JAR simulations. (A) 3D representation of ΔATP on amplitude and baseline frequency in +5 Hz jamming. (B) Heat map of ΔATP on amplitude and baseline frequency in +5 Hz jamming. (C) 3D representation of ΔATP on amplitude and baseline frequency in -5 Hz jamming. (D) Heat map of ΔATP on amplitude and baseline frequency in -5 Hz jamming. (E) 3D representation of ΔATP on amplitude and baseline frequency in +10 Hz jamming. (F) Heat map of ΔATP on amplitude and baseline frequency in +10 Hz jamming. (G) 3D representation of ΔATP on amplitude and baseline frequency in -10 Hz jamming. (H) Heat map of ΔATP on amplitude and baseline frequency in -10 Hz jamming.

Figure 1

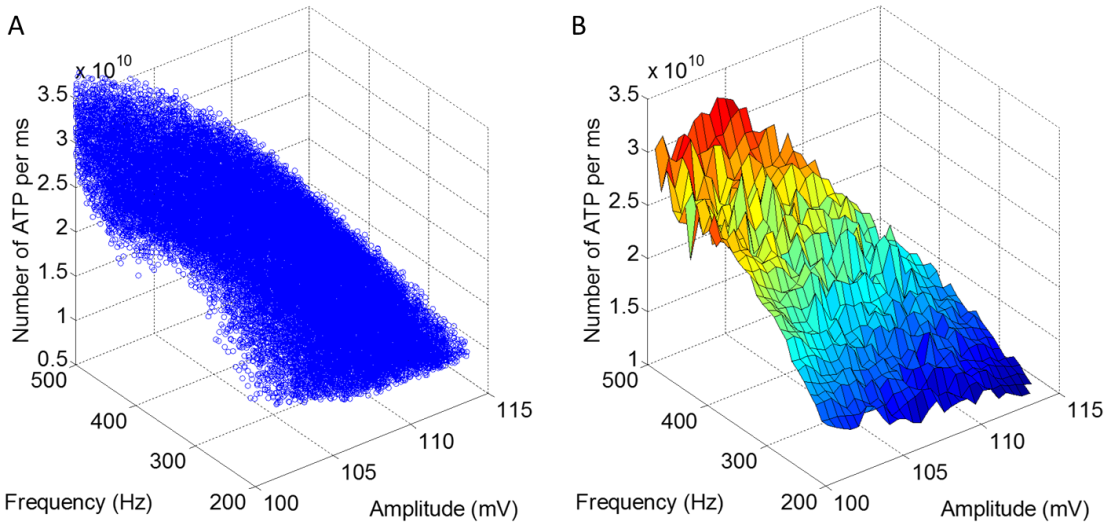
A
x 10^10
3.5
3
2.5
2
1.5
1
0.5
Number of ATP per ms
500
400
300
200
Frequency (Hz)
100
105
110
115
Amplitude (mV)
B
x 10^10
3.5
3
2.5
2
1.5
1
Number of ATP per ms
500
400
300
200
Frequency (Hz)
100
105
110
115
Amplitude (mV)

Figure 2

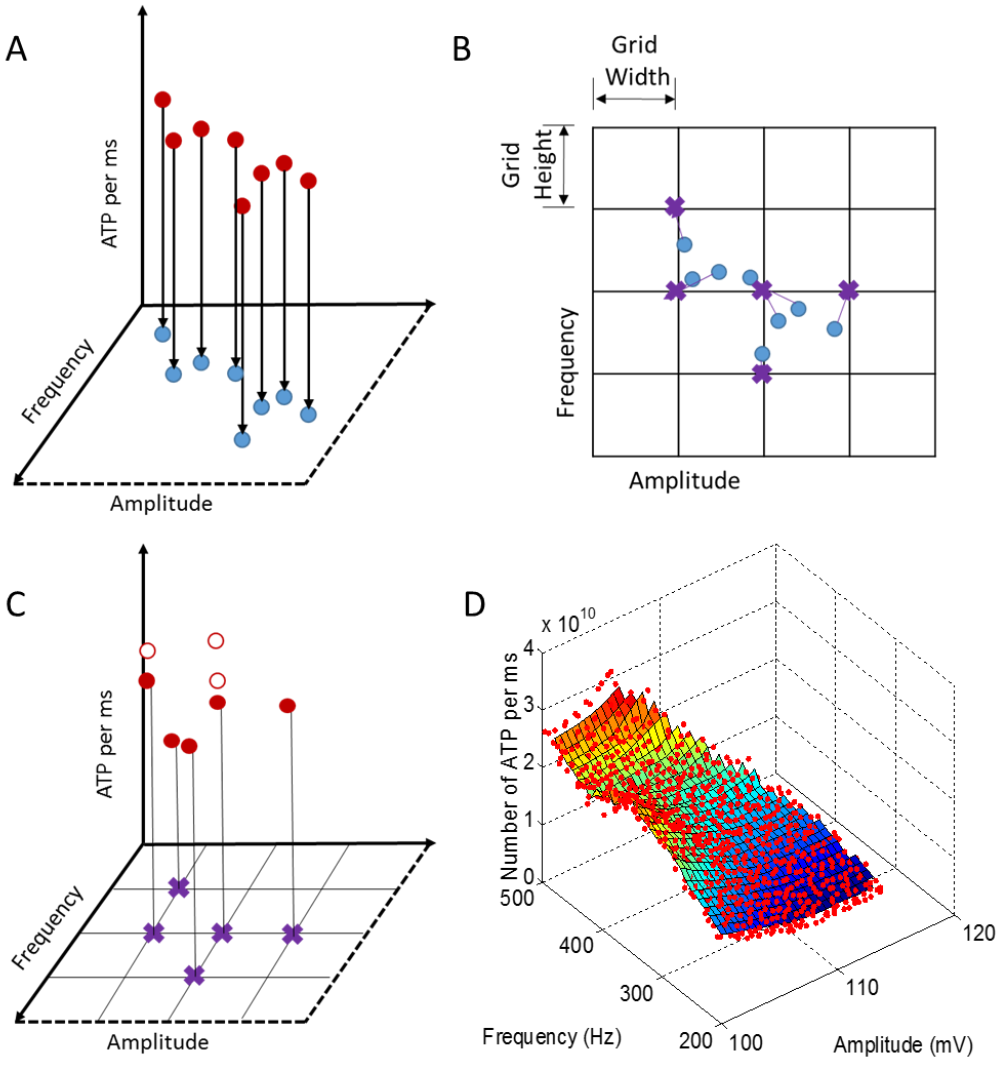
A
ATP per ms
Frequency
Amplitude
B
Grid
Width
Grid
Height
Frequency
Amplitude
C
ATP per ms
Frequency
Amplitude
D
x 10^10
Number of ATP per ms
4
3
2
1
0
500
400
300
200
Frequency (Hz)
100
110
120
Amplitude (mV)

Figure 3

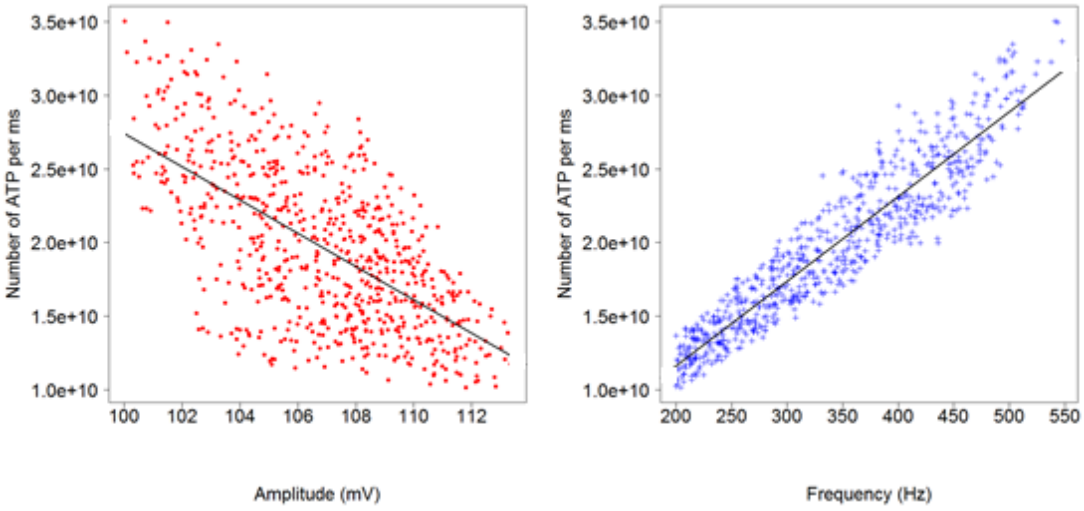
3.5e+10
3.0e+10
2.5e+10
2.0e+10
1.5e+10
1.0e+10
Number of ATP per ms
100
102
104
106
108
110
112
Amplitude (mV)
200
250
300
350
400
450
500
550
Frequency (Hz)

Figure 4

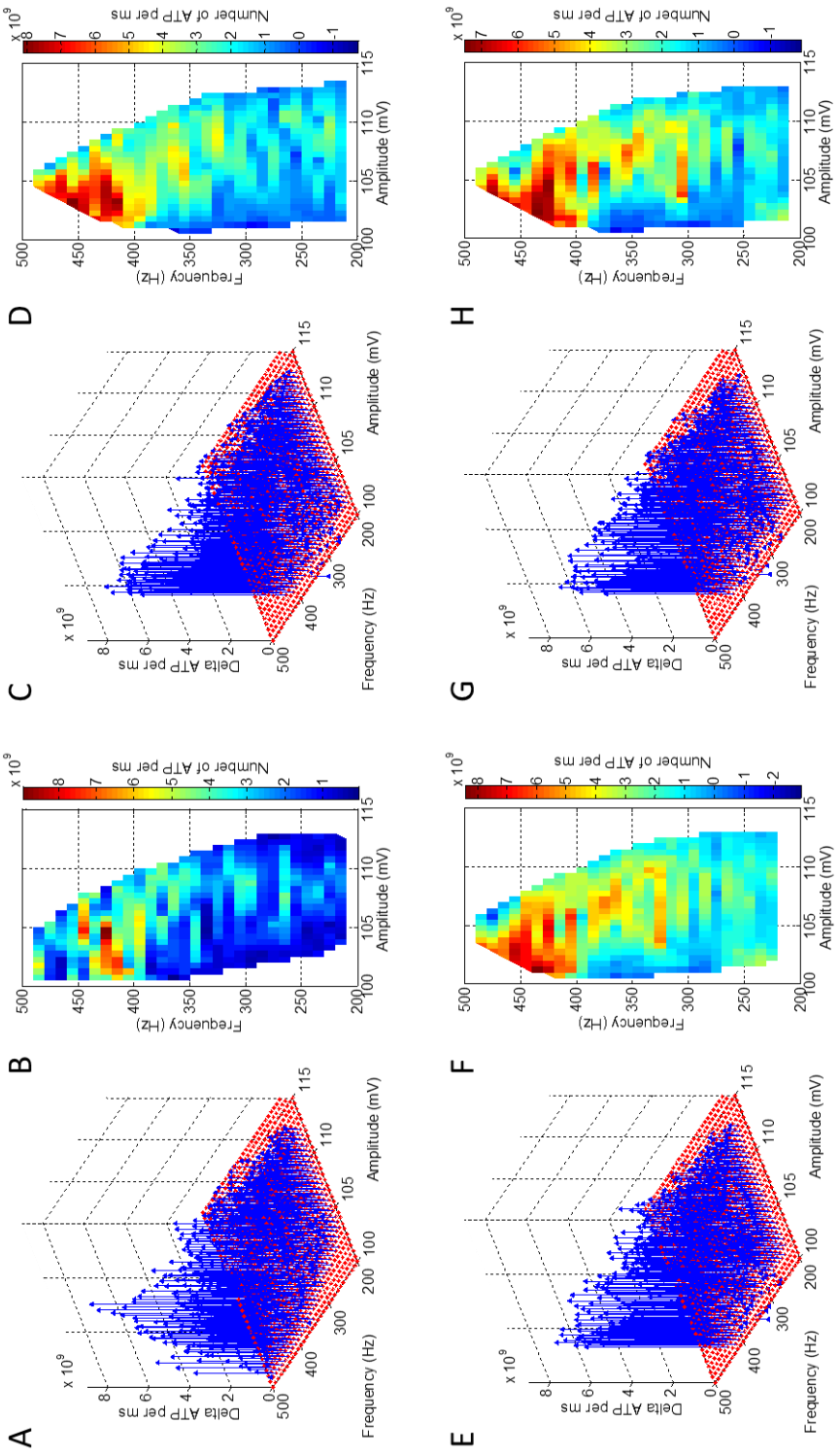
A
B
C
D
E
F
G
H
Delta ATP per ms
Number of ATP per ms
Frequency (Hz)
Amplitude (mV)
x 10^9

Chapter 3: Signaling Behavior Experiments

Introduction

Weakly electric fish generate electric signals to image their world and communicate with conspecifics in dark and murky waters. Some gymnotiform species produce regular EODs constantly without interruption, incurring very high metabolic costs that in some cases are comparable to the most energetically expensive animal communication signals such as trilling katydids and Carolina wrens (Lewis et al., 2014; Markham et al., 2016; Salazar and Stoddard, 2008; Stoddard and Salazar, 2010). *E. virescens* is a weakly electric fish that produces quasi-sinusoidal EODs at constant frequencies ranging from 200 to 600 Hz (Scheich, 1977). They are distributed in the rivers of central South America, where they shoal in large social groups (Albert and Reis, 2011).

Communication signals with high amplitude and high frequency often confer advantages such as greater advertisement to potential mates, increasing ability to warn conspecifics for territorial defense and stronger sensory stimulation to receiving individuals (Stoddard and Salazar, 2011). For *E. virescens*, EODs of high amplitude and high frequency also provide more information from the surrounding environment and enable more accurate sensory performance. Higher frequency EODs provide more rapid sampling of the sensory environment, while high-amplitude EODs serve to expand the sensory volume surrounding the fish. However, large metabolic costs arising from electric signals with both high amplitude and high frequency potentially would counteract the benefits that they bring.

Amplitude and frequency are two key EOD features believed to determine the energetic costs of generating the signals (Salazar et al., 2013; Lewis et al., 2014). *E.*

virescens are known to transiently change both EODa and frequency in response to environmental conditions. For instance, *E. virescens* change EODa on a circadian rhythm, increasing amplitude at night when these nocturnal fish are active and decreasing EODa during the day when fish are at rest (Sinnett and Markham, 2015). *E. virescens* also decrease signal amplitude over a period of days during food deprivation and restores the original signal amplitude within two days once feeding resumes (Sinnett and Markham, 2015). Rapid decreases in EODa also occur in response to hypoxia (Reardon et al., 2011).

Transient changes in EODf occur during the jamming avoidance response (JAR). The presence of a neighboring conspecific with an EODf similar frequency to the fish's EODs can interfere with the sensory signal and impair electrolocation effectiveness. To resolve this, when two electric fish with similar frequencies are in close proximity, the fish with the slightly higher frequency further increases its frequency by ~5-10 Hz and the other fish with a slightly lower frequency will decrease its frequency by ~5-10 Hz. This frequency modulation enables the fish to avoid signal jamming and maintain the effectiveness of sensory performance. The computational simulations from Chapter 2 predict that signal frequency has a strong positive effect on energetic costs of generating the electric signal, a conclusion consistent with recent experimental findings (Lewis et al., 2014). Presumably raising EODf during the JAR incurs higher energetic costs while the reduced EODf of the second fish decreases its sensory sampling rate, potentially compromising sensory performance.

Given that *E. virescens* exhibits changes in both EODa and EODf in response to environmental conditions, this fact raises the question of whether energetic limitations

and sensory performance might force a tradeoff in one parameter if the other changes. For example, if a fish increases EODf during a JAR, is there a corresponding decrease in EODa to offset the increased metabolic cost incurred by a higher EODf? Conversely, if environmental conditions elicit a decrease in EODf, will there be a corresponding increase in EODa? I therefore hypothesized that during JAR, fish exposed to jamming stimuli that increased EODf (up-jamming) would decrease EODa to conserve energy while fish exposed to jamming stimuli that decreased EODf (down-jamming) would increase EODa to compensate for the loss in sensory resolution.

In this study, I also explored whether environmental conditions that require increases in EODa would produce compensatory changes in EODf. When electric fish inhabit waters near centers of human population, stray electrical noise from power transmission lines creates broadband electrical noise in the water (Joerg Henninger, personal communication). Presumably, stronger background noise decreases the EOD signal-noise ratio and impairs the efficacy of signal propagation. It is very likely that electric fish living in electrically noisy environments could increase EODa to overcome the background electrical noise, just as birds in noisy urban environments emit higher-amplitude calls (Nemeth et al., 2013).

No study to date has reported the effect of electric noise on signaling behavior of weakly electric fish. White noise is a standardized form of electric noise with a uniform power distribution across the frequency domain. In the presence of electrical white noise, the signal efficacy of weakly electric fish should be impaired but they cannot overcome this noise by shifting their EODf away from the noise as is the case during the JAR. I hypothesized that when *E. virescens* is exposed to white noise, fish would

increase EODa to compensate for the decrease in signal-noise ratio and would decrease EODf to compensate for the increased metabolic costs of higher EODa.

Methods

Animals

Wild-caught *E. virescens* (Glass knife-fish) from tropical South America were purchased from a tropical fish supplier. Fish were kept in groups of 4 to 10 individuals in 40- or 10-liter tanks within a recirculating aquarium system. The system temperature was maintained at 28 ± 1°C and the water conductivity was kept at 200-500 μS/cm. *E. virescens* generate sinusoidal EOD waveforms with a frequency of 200-600 Hz (Fig. 1D). Each positive pulse is counted as a single EOD (Fig. 1C). The EOD is regulated by a medullary pacemaker nucleus (Fig. 1A,B). Eight fish ranging from 17 to 24 cm and 13.1 to 20.2 g, obtained from 5 different tanks, were used in this experiment. All methods were approved by the Institutional Animal Care and Use Committee of The University of Oklahoma, and complied with the Public Health Service Guide for the Care and Use of Laboratory Animals.

Experimental Procedures

The experiment was conducted in an automated measurement tank (Fig. 1E), 120 x 44 x 44 cm, located in a light- and temperature-controlled room on a 12L:12D light cycle. Fish were allowed to acclimate to the recording tanks for at least 24 hours prior to beginning each experiment. During the experiment, fish were restricted in an electrically-transparent mesh tube centered within the tank. The EOD waveform was amplified from nichrome wire electrodes at opposite ends of the tank. EODa was measured peak-to peak and EODf was computed from waveform zero crossings during

each 100-ms sample. EODs were recorded throughout each experiment at intervals of approximately 10s.

Jamming and white noise stimulus presentation and data acquisition were controlled by a custom EOD recording system coded in RPvdsEX (Alachua, Florida) and Matlab (Mathworks, Inc. Natick MA). EODs were amplified by Cyngus Technologies FLA01 amplifiers (Delaware Water Gap, PA). Inputs were AC coupled and amplified at 500x gain with 12.5 kHz high-pass filtering. A Tucker Davis Technologies RX8 multi I/0 processor (Alachua, Florida) was used to digitize recorded EODs and to generate the stimulus signals with a sampling rate of 48 kHz. The jamming stimulus was a bipolar sine wave produced by the RX8 processor, isolated from chassis ground by an A-M systems Analog Stimulus Isolator Model 2200 (Sequim, WA), and delivered to the experimental tank via 3-cm nichrome wires 20 cm apart on either side of the fish (orthogonal to the recording electrode axis). The experimental control platform was established via a custom graphical user interface coded in Matlab (Mathworks, Inc. Natick MA). The output stimulus was calibrated so that the jamming and white noise stimulus amplitudes were maintained at 1.0 and 3.0 mV/cm, respectively, during stimulation. The frequency of the jamming stimulus was set to 3 Hz above or 3 Hz below the fish's recorded frequency at the beginning of the stimulus period. During periods of stimulus delivery, EOD signals were recorded during 100 ms interruptions in the stimulus signal so that EOD recordings were not contaminated by stimulus signal. A Tektronix TDS 2024C oscilloscope (Beaverton, OR) was used to monitor real-time waveforms of stimulus and recorded EODs.

Experimental trials consisted of 60 min baseline EOD recordings, followed by 90 min of stimulus presentation, then by at least 60 min of recovery after termination of the stimulus. Each fish was exposed to all three stimulus conditions on separate days: white noise, up-jamming (stimulus frequency 3 Hz below fish's frequency), or down-jamming (stimulus frequency 3 Hz above fish's frequency).

Data analysis

To quantify the rate and direction of changes in EODa at key time points in the experiments, the linear slope of EODa was compared across 4 different intervals (Fig. 2A). The 20 minutes before stimulus initiation was denoted as *Baseline*. The 20 minutes immediately following stimulus initiation was denoted as *Stimulus 1*. The last 20 minutes of stimulus presentation was identified as *Stimulus 2*, and the first 20 minutes of the recovery period was defined as *Recovery*. Simple linear regression was used to determine the rate of change in EODa for all four intervals. To account for differences in baseline EODa among fish, the regression slopes for all intervals were normalized to the mean EODa during the Baseline interval.

The magnitude of stimulus-induced changes in EODa (ΔAmp) during the stimulus presentation were compared to changes in EODa during the 60 min prior to stimulus onset. *Control* condition ΔAmp was computed as the difference between mean EODa in the 20-min interval beginning 70-min before stimulus onset (*Prebaseline EODa*) and the mean EODa in the 20-min interval before stimulus onset (*Onset EODa*) (Fig. 2B). *30-min-Stimulus* condition ΔAmp was computed as the difference between mean EODa in the 20-min interval beginning 30 min after stimulus onset (*Stimulus 30min EODa*) and *Onset EODa*. *Final-Stimulus* condition ΔAmp was computed as the

difference between mean EODa in the final 20-min interval of stimulus presentation (*Stimulus Final EODa*) and *Onset EODa.* All ΔAmp values were normalized to *Onset EODa*. Statistical analysis and data visualization were conducted using R (The R Foundation for Statistical Computing, Vienna, Austria) and Matlab (Mathworks, Inc. Natick MA).

Results

The introduction of down-jamming and up-jamming stimuli (3 Hz above and below the baseline frequency, respectively) caused an observable jamming avoidance response in 8 out of 8 fish (down-jamming) and 7 out of 8 fish (up-jamming)(Appendix B1,B2). Increases in EODa were observed in many, but not all fish (7 out of 8 in up-jamming tests and 6 out of 8 in down-jamming tests), but in no case did EODa decrease (Appendix C1,C2). In the white noise experiments, a similar pattern of amplitude change was detected where EODa increased in 7 out of 8 fish (Appendix C3). However, two different patterns of frequency change were observed. Three out of 8 (Appendix B3) fish decreased frequency during the white noise stimulus, while the other 5 fish showed small and unsystematic fluctuations of frequency around their baseline frequency.

To track the tendency of amplitude change, regression slopes of the four time periods: *Baseline*, *Stimulus 1*, *Stimulus 2* and *Recovery* in experiments with different stimuli, standardized by the baseline amplitude, were computed and compared. A consistent pattern in up-jamming, down-jamming and white-noise stimulation was that the slope of amplitude measurement increased from approximately zero at *Baseline*, to positive values at *Stimulus 1*, dropped to zero at *Stimulus 2*, then decreased to negative

values during *Recovery* (Fig. 3). Repeated measures ANOVA revealed significant difference in the slopes of the four time periods during all three stimulus types: up-jamming ($p = 0.03$), down-jamming ($p = 0.003$) and white-noise ($p = 0.02$). Subsequent Tukey's pairwise comparisons revealed significant steeper standardized slopes of *Stimulus 1* than those of *Recovery* for all three stimulation types ($p = 0.02$ for up-jamming, $p = 0.002$ for down-jamming, $p = 0.01$ for white-noise), while in down-jamming, significant difference in slope values was also identified between Stimulus2 and Recovery ($p = 0.02$).

EODa increased at *Stimulus 30 min* and *Stimulus Final* across all three stimulus types. ΔAmp of *Final-Stimulus* condition was significantly larger than Control for all the three types of stimulus (Fig. 4): up-jamming (repeated measure ANOVA, $p = 0.01$, Tukey's pairwise test, $p = 0.002$), down-jamming (repeated measure ANOVA, $p = 0.006$, Tukey's pairwise test, $p < 0.001$) and white-noise (repeated measure ANOVA, $p = 0.006$, Tukey's pairwise test, $p < 0.001$). ΔAmp of *30-min-Stimulus* was also higher than *Control* but statistical significance was not detected at all three stimulus types (Tukey's pairwise test, $p = 0.08$ for up-jamming, $p = 0.02$ for down-jamming and $p = 0.006$ for white-noise).

Discussion

In the present experiment, I exposed *E. virescens* to stimuli designed to produce changes in EODf or changes in EODa. Contrary to my hypothesis, increases in EODf did not cause decreases in EODa, and increases in EODa were not accompanied by decreases in EODf. Both upward and downward changes in EODf were accompanied by increased EODa during the JAR experiments. In the presence of white noise,

changes in EODf were small and unreliable in 5 of 8 fish, but I did observe clear changes in EODa, with three cases where EODf decreased.

I hypothesized that fish that increased EODf during the JAR would decrease EODa to conserve energy. However, the results of the up-jamming condition showed considerably higher amplitude at stimulus compared with baseline. The increased slope of EODa immediately after stimulus onset suggests that this change in EODa is a rapid response to the stimulus. Based on this result, my hypothesis was not supported because EODa changed in the opposite direction than I had predicted. One possible explanation is that the positive shift of around 5 to 10 Hz in EODf indeed incurred additional energetic demand but not enough to reach an energetic constraint that would force a tradeoff in EODa. Thus the fish would be able to accommodate the increased energetic demands without reducing EODa. Another alternative interpretation is that EODa does not have as much of an impact on energetic costs as does EODf. This interpretation is consistent with the results of the computational studies from Chapter 2 of this thesis. Within these simulations, no clear relationship was found between EODa and energetic costs of producing EOD at the cellular level, and the marginal effect of EODa even showed a slightly negative effect on metabolic demands.

In the down-jamming condition, fish reduced EODf as expected. The reduction of EODf would be expected to reduce energetic demands, thus energetic constraints would be no more of a determinant factor of the signal modulation in this case. However, the frequency drop here could impair sensory performance of the fish because signal features are closely related to image distance and resolution in electrolocation as well as the quality and efficacy of electrocommunication. So it was reasonable to

hypothesize that the fish decreasing EODf during JAR would increase its EODa to compensate for signal efficacy. The results of the down-jamming experiments indeed revealed a significant increase in EODa. Additionally, the slope of EODa increased immediately after stimulus onset and decreased immediately after stimulus termination.

When electric noise is present in the environment of weakly electric fish, the efficacy of signaling should decrease because of a degraded signal-to noise ratio. Accordingly, I hypothesized that when exposed to broad-band white noise, *E. virescens* would raise its EODa to maintain a relatively high signal-noise ratio and would reduce its EODf to offset the metabolic costs of increased EODa. This hypothesis was based on the assumption that EODa was positively related to signal energetic costs. However the simulation experiments from Chapter 2 of this thesis predicted a slightly negative correlation between signal amplitude and the ATP consumption of producing EODs. So even though an increase of EODa was observed when fish were exposed to white noise, the hypothesis itself cannot well explain the mechanism. Moreover, the frequency pattern was divergent in that some fish (3 out of 8) displayed a decrease in frequency and the others did not, indicating that an urgent requirement to conserve energy did not affect all fish. This outcome is consistent, to a certain degree, with the unclear effect of signal amplitude on energetic costs observed in the simulation studies of Chapter 2.

While the results revealed some patterns in both amplitude and frequency response of *E. virescens* exposed to stimulus, the behavior experiments here have some limitations. Firstly, only eight fish were tested under each type of stimulus. The small sample size might reduce the statistical power of the study and raise the margin of error. Secondly, all the behavior tests were conducted during the day (light cycles). The

purpose of this was to reduce unreliable signal recording caused by body movement of test fish since they are more active at night. However, the presence of light might introduce bias and the results may not well reveal the signal response pattern to stimulus during dark cycles. These limitations should be taken into consideration in the experiment design of future study.

In conclusion, tradeoff between EODa and EODf was observed in only the down-jamming and some white-noise tests. No tradeoff was detected in up-jamming tests, where I expected fish to show a co-effect of both energetic limitations and sensory efficacy on signal modulation. Taken as a whole, the present results indicate that our understanding of energetic constraints on EOD signaling in *E. virescens* is far from complete. While convincing experimental outcomes demonstrate that EOD signaling is compromised under metabolic stress, and that EOD signaling consumes a significant fraction of the energy budget, the present data resulting from short-term perturbations in EODa and EODf suggest that signal energetics are not limiting in all conditions. Further research is needed to fully specify the conditions under which metabolic factors influence EOD signaling across timescales ranging from seconds to month.

Figures

Figure 1: The electric organ discharge (EOD) in *E. virescens*. (A) The medullary pacemaker nucleus innervates electrocytes of the electric organ through spinal motor neurons. The synchronous action potentials in the electric organ produce the EOD. (B) Electrocytes produce action potentials simultaneously, with the current flow summing in the direction of the head. The returning path of the current flow is towards the tail. (C) The voltage potential trace of 1 EOD pulse. (D) The waveform of continuous EODs at ~500 Hz. (E) A sketch diagram of the experimental apparatus. **(**Adapted from Sinnett and Markham, 2015)

Figure 2: Different time periods of behavior experiments involved in the computation and statistical analysis. (A) Schematic illustration of the four intervals: *Baseline, Stimulus 1, Stimulus 2* and *Recovery,* from which the standardized regression slopes were computed. (B) Schematic illustration of the four time periods: *Prebaseline, Onset, Stimulus 30min* and *Stimulus Final* from which the control and tested conditions (*30-min-Stimulus* and *Final-Stimulus*) were defined.

Figure 3: Standardized amplitude slopes of the four different intervals: *Baseline, Stimulus 1, Stimulus 2* and *Recovery*. The upper, middle and lower panels represent the effects of up-jamming, down-jamming and white-noise stimulus, respectively. Significance at $p < 0.05$ marked as "*".

Figure 4: Grouped bar plots that compare ΔAmp between *30-min-Stimulus, Final-Stimulus* and *Control* during all three stimulus types: down-jamming, up-jamming and white-noise. Significance were detected between different letters (a and b) within each group.

Figure 1

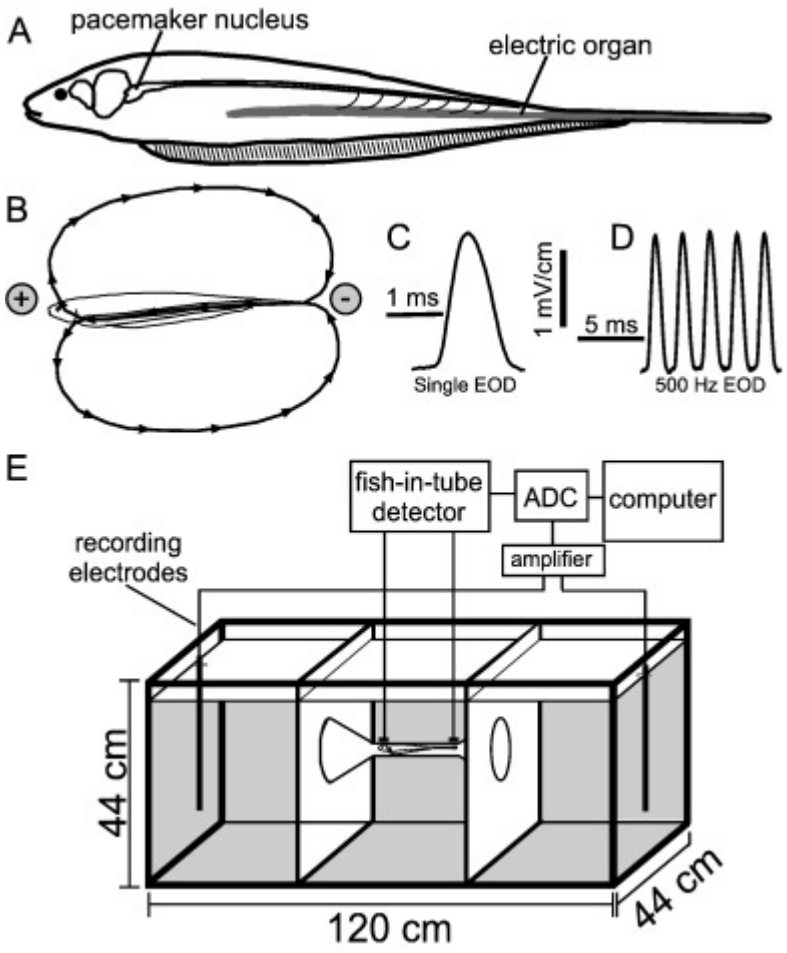
A
pacemaker nucleus
electric organ
B
+
-
C
1 ms
1 mV/cm
Single EOD
D
5 ms
500 Hz EOD
E
fish-in-tube detector
ADC
computer
amplifier
recording electrodes
44 cm
120 cm
44 cm

Figure 2

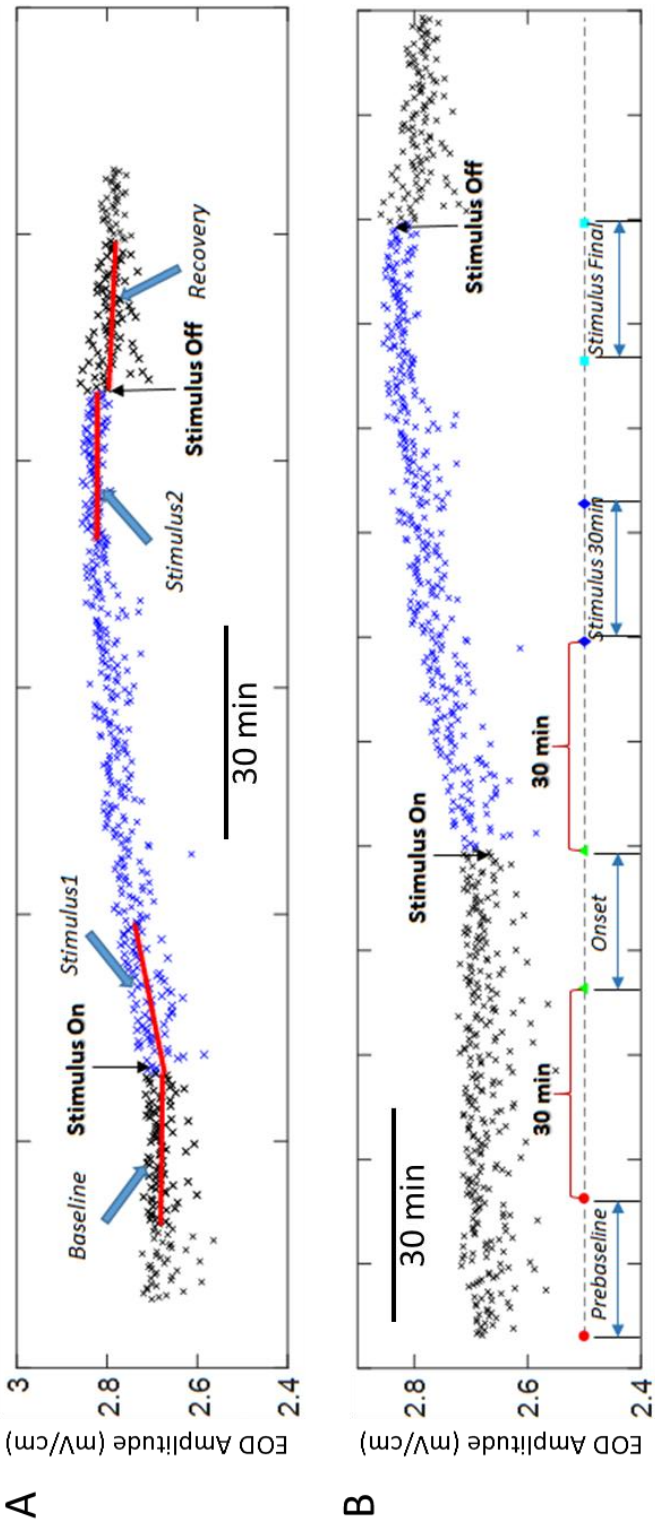
A
B
EOD Amplitude (mV/cm)
3
2.8
2.6
2.4
Baseline
Stimulus On
Stimulus1
Stimulus2
Stimulus Off
Recovery
30 min
Prebaseline
Onset
Stimulus 30min
Stimulus Final
30 min
30 min

Figure 3

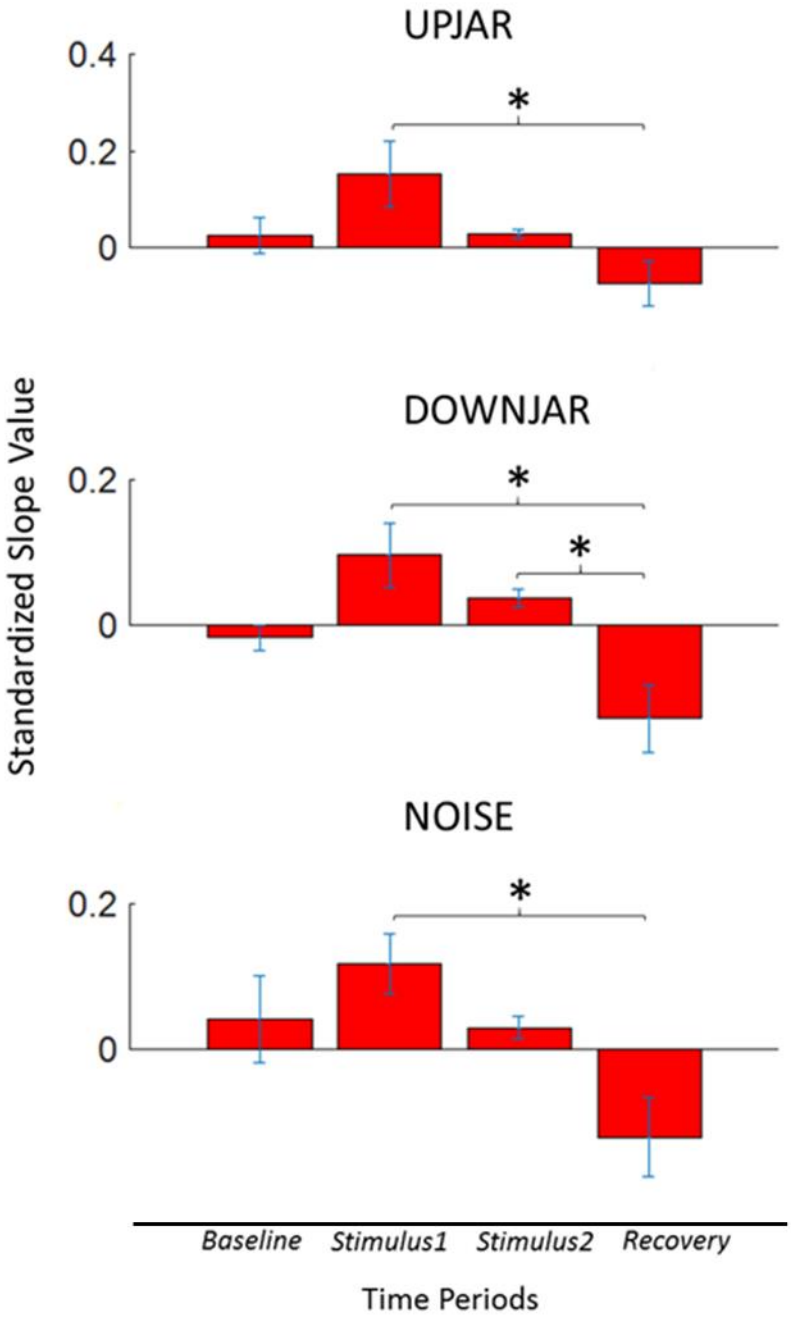
UPJAR
0.4
0.2
0
*
DOWNJAR
0.2
0
*
*
NOISE
0.2
0
*
Standardized Slope Value
Baseline
Stimulus1
Stimulus2
Recovery
Time Periods

Figure 4

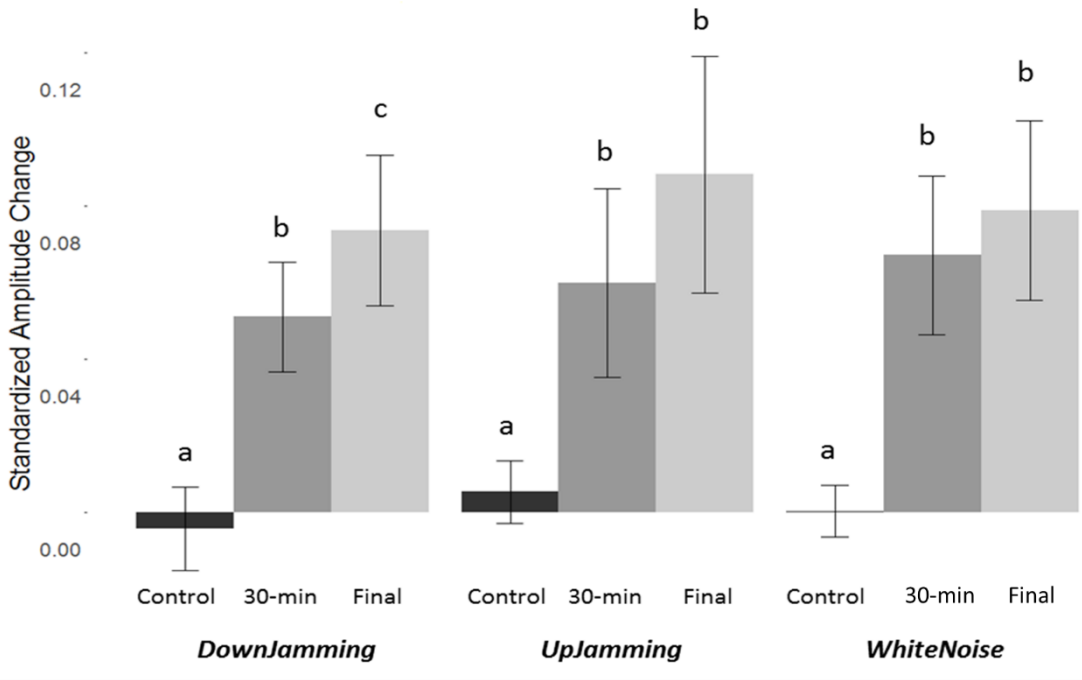
Standardized Amplitude Change
0.12
0.08
0.04
0.00
a
b
c
a
b
b
a
b
b
Control
30-min
Final
Control
30-min
Final
Control
30-min
Final
DownJamming
UpJamming
WhiteNoise

Chapter 4: Summary and Future Directions

Weekly electric fish produce electric organ discharges (EODs) for the purpose of both sensing their environment and communication. As for all the other communication modalities, this electric signaling system evolved under selective pressures to balance the benefits and costs associated with the signaling behavior. While discharging with higher intensity and higher frequency provides the fish with an expanded sensory range, clearer images of the surrounding environment, and better quality of communication with conspecifics, it also exposes them to electroreceptive predators and requires a larger energetic investment. The research reported in this thesis focused on how the energetic costs of the electric signal might affect signaling behaviors of weakly electric fish.

EODs are energetically expensive to produce. Previous theoretic studies estimated that production of EOD signals could cost up to ~30% of the daily energy budget in wave-type fish which produce constant regular discharge (Salazar and Stoddard, 2008; Lewis et al., 2014), and this prediction was confirmed in recent experimental studies (Markham et al., 2013; Salazar et al., 2013). *E. virescens* is an example of wave-type fish that can produce EODs with a frequency as high as 600 Hz, and cost ~1-3 × 10^{10} ATP per EOD in a single electrocyte (Lewis et al., 2014). Signal features such as amplitude and frequency were thought to be related with energetic costs associated with EOD production. A recent simulation study showed that maintaining EODa at higher frequency required larger energetic costs (Lewis et al., 2014). The goal of the present project was to explore the effect of signal amplitude and frequency on signaling energetic costs and investigate how energetic constraints

induced by amplitude or frequency increase influenced signaling behavior in weakly electric fish *E. virescens.*

In the computational studies in Chapter 2, EODf was positively related with energetic costs in the *Eigenmannia* electrocyte; higher EODf required drastically more ATP molecules per unit time. The simulation of the JAR within these simulations also revealed that frequency shifts at higher baseline frequencies caused larger deviations from optimal energetic efficiency, further confirming the importance of EODf to signal energetics. However, no clear effect of EODa on metabolic costs was identified. It appeared, based on these simulations, that frequency might be more closely related with energetic costs of EOD production than amplitude. This result did not support my original hypothesis and also failed to explain the amplitude decrease observed under hypoxia or food deprivation, which were considered to be conditions of energetic constraint.

One alternative interpretation is that the two features, frequency and amplitude, were not able to provide sufficient information to the model and resulted in underfitting of the model. It is also likely that the model itself is missing important components and needs to be further developed. As for future work, continuous efforts to re-evaluate and optimize the electrocyte computational model are necessary. In the meantime, it is likely worthwhile to introduce other signal features into the prediction model. One possible candidate feature is the shape of the EOD waveform. In signal processing, continuous electric potential measurements are used to compute the power and energy of an electric signal, indicating that the shape of the waveform is also involved in determining signal energy, besides the peak-to-peak amplitude.

Though the signal energy in this context is not exactly the same as the physical energetic costs as we mentioned above, the two concepts are closely related and it is possible to convert from one to the other with certain mathematical operations. With some appropriate method of quantifying the shape of signal waveforms, it will be possible extract one or more variables associated with the shape and introduce them into the prediction model. Skewness and kurtosis are two candidate variables to represent the signal shape. Once more information is provided from these extra features, perhaps the pattern of signal amplitude on signal metabolic cost could become clearer.

The behavioral experiments in Chapter 3 tested for potential tradeoffs between signal amplitude and frequency. The up-jamming stimulus caused fish to increase both amplitude and frequency. If the amplitude is positively related to signaling costs, then the observed amplitude increases that accompanied increased frequency might indicate that energetic demands introduced by frequency shifts in JAR are small enough that the fish was still able to balance the extra metabolic costs without sacrificing signal intensity. However, the positive correlation between EODa and energetic demands was not verified in the computational simulations, so it is possible that the fish modulate signal features via a different mechanism in response to the stimulus. Tradeoff of amplitude increase and frequency drop was identified in down-jamming experiments. This finding lends some support to my hypothesis that fish might increase EODa to compensate for decreased EODf, which might maintain signal quality and its adaptive benefits. In the white-noise experiments, I expected to observe increased EODa and decreased EODf based on the expectation that fish would increae EODa to maintain a relatively high signal to noise ratio for signal efficacy, with a drop in EODf to conserve

energy. Though EODa did increase during the white-noise stimulus, there was no consistent decrease in EODf. A reduction in EODf was only observed in 3 out 8 fish in response to broad-band white noise, possibly because increased EODa imposes little additional metabolic cost – an interpretation consistent with my findings from Chapter 2. In future research, it will be worthwhile to experimentally verify the relationship between EODa and energetic demands of generating the signal, perhaps through whole-animal respirometry experiments. In addition, more acute and severe energetic challenges beyond those imposed by the JAR or white-noise stimulation might be needed to observe the potential tradeoff between EODa and EODf.

The present sstudy provides a good starting point for further investigation of the energetics of EOD production and any corresponding energetic constraints. Future research should attempt to develop better elaborated computational models that could provide theoretical insights on the basis of signal feature modulation in weakly electric fish. In addition, more experimental evidence is needed concerning the ways in which signal energetics affect signaling behavior in weakly electric fish. Continued integration of theoretical and computational models with expanding experimental data in this area promises to better elucidate the causes and mechanisms underlying the ways in which animals regulate their communication signals to balance the costs and benefits associated with signaling.

References

Albert, J.S. and Reis, R. eds., 2011. *Historical biogeography of Neotropical freshwater fishes*. Univ of California Press.

Albert, J.S. and Crampton, W.G., 2005. Diversity and phylogeny of Neotropical electric fishes (Gymnotiformes). In *Electroreception* (pp. 360-409). Springer New York.

Amidror, I., 2002. Scattered data interpolation methods for electronic imaging systems: a survey. *Journal of electronic imaging*, *11*(2), pp.157-176.

Attwell, D. and Laughlin, S.B., 2001. An energy budget for signaling in the grey matter of the brain. *Journal of Cerebral Blood Flow & Metabolism*, *21*(10), pp.1133-1145.

Ban, Y., Smith, B.E. and Markham, M.R., 2015. A highly polarized excitable cell separates sodium channels from sodium-activated potassium channels by more than a millimeter. *Journal of neurophysiology*, *114*(1), pp.520-530.

Bean, Bruce P. "The action potential in mammalian central neurons." *Nature Reviews Neuroscience* 8.6 (2007): 451-465.

Bennett, M.V., 1970. Comparative physiology: electric organs. *Annual review of physiology*, *32*(1), pp.471-528.

Bradbury, J.W. and Vehrencamp, S.L., 1998. Principles of animal communication.

Bullock, T.H., Hamstra Jr, R.H. and Scheich, H., 1972. The jamming avoidance response of high frequency electric fish. In *How do Brains Work?* (pp. 509-534). Birkhäuser Boston.

Carlson, B.A. and Kawasaki, M., 2007. Behavioral responses to jamming and 'phantom'jamming stimuli in the weakly electric fish Eigenmannia. *Journal of Comparative Physiology A*, *193*(9), pp.927-941.

Carter, B.C. and Bean, B.P., 2009. Sodium entry during action potentials of mammalian neurons: incomplete inactivation and reduced metabolic efficiency in fast-spiking neurons. *Neuron*, *64*(6), pp.898-909.

Endler, J.A., 1992. Signals, signal conditions, and the direction of evolution. *The American Naturalist*, *139*, pp.S125-S153.

Endler, J.A., 1993. Some general comments on the evolution and design of animal communication systems. *Philosophical Transactions of the Royal Society B: Biological Sciences*, *340*(1292), pp.215-225.

Heiligenberg, W., 1973. Electrolocation of objects in the electric fishEigenmannia (Rhamphichthyidae, Gymnotoidei). *Journal of Comparative Physiology A: Neuroethology, Sensory, Neural, and Behavioral Physiology*, *87*(2), pp.137-164.

Hopkins, C.D., 1999. Design features for electric communication. *Journal of experimental Biology*, *202*(10), pp.1217-1228.

Howarth, C., Gleeson, P. and Attwell, D., 2012. Updated energy budgets for neural computation in the neocortex and cerebellum. *Journal of Cerebral Blood Flow & Metabolism*, *32*(7), pp.1222-1232.

Joos, B., Markham, M.R., Steimle, Y., Lewis, J.E., Catherine, M.E. 2016. Modeling the oscillating dipole properties of electric organ discharge in the weakly electric fish, *Eigenmannia*. *Biophys. J*. (YEAR): 110, 631a.

Kirchner, W.H. and Dreller, C., 1993. Acoustical signals in the dance language of the giant honeybee, Apis dorsata. *Behavioral ecology and sociobiology*, *33*(2), pp.67-72.

Krahe, R., Maler, L. 2014. Neural maps in the electrosensory system of weakly electric fish. *Curr. Opin. Neurobiol.* 24, 13-21.

Leech, S.M. and Leonard, M.L., 1997. Begging and the risk of predation in nestling birds. *Behavioral Ecology*, *8*(6), pp.644-646.

Lewis, J.E., Gilmour, K.M., Moorhead, M.J., Perry, S.F. and Markham, M.R., 2014. Action potential energetics at the organismal level reveal a trade-off in efficiency at high firing rates. *Journal of Neuroscience*, *34*(1), pp.197-201.

Marder, E. and Goaillard, J.M., 2006. Variability, compensation and homeostasis in neuron and network function. *Nature Reviews Neuroscience*, *7*(7), pp.563-574.

Markham, M.R. 2013. Electrocyte physiology: 50 years later. *Journal of Experimental Biology* 216, 2451-2458.

Markham, M.R., Ban, Y., McCauley, A.G. and Maltby, R., 2016. Energetics of Sensing and Communication in Electric Fish: A Blessing and a Curse in the Anthropocene?. *Integrative and comparative biology*, p.icw104.

Markham, M.R., Kaczmarek, L.K., Zakon, H.H., 2013. A sodium-activated potassium channel supports high-frequency firing and reduces energetic costs during rapid modulations of action potential amplitude. *Journal of Neurophysiology* 109, 1713-1723.

Markham, M.R., McAnelly, M.L., Stoddard, P.K., Zakon, H.H. 2009. Circadian and social cues regulate ion channel trafficking. *PLoS Biology*. 7, e1000203.

Moller, P., 1970. ‘Communication’in weakly electric fish, Gnathonemus niger (mormyridae) I. Variation of electric organ discharge (EOD) frequency elicited by controlled electric stimuli. *Animal Behaviour*, *18*, pp.768-786.

Moller, P. and Bauer, R., 1973. ‘Communication’in weakly electric fish, Gnathonemus petersii (Mormyridae) II. Interaction of electric organ discharge activities of two fish. *Animal Behaviour*, *21*(3), pp.501-512.

Nelson, M.E. and MacIver, M.A., 2006. Sensory acquisition in active sensing systems. *Journal of Comparative Physiology A*, *192*(6), pp.573-586.

Nemeth, E., Pieretti, N., Zollinger, S.A., Geberzahn, N. and Partecke, J., 2013. Bird song and anthropogenic noise: vocal constraints may.

Parker, G.A. and Smith, J.M., 1990. Optimality theory in evolutionary biology. *Nature*, *348*(6296), pp.27-33.

Reardon, E.E., Parisi, A., Krahe, R. and Chapman, L.J., 2011. Energetic constraints on electric signalling in wave-type weakly electric fishes. *Journal of Experimental Biology*, *214*(24), pp.4141-4150.

Salazar, V.L., Krahe, R., Lewis, J.E. 2013. The energetics of electric organ discharge generation in gymnotiform weakly electric fish. *Journal of Experimental Biology* 216, 2459-2468.

Salazar, V.L., Stoddard, P.K. 2008. Sex differences in energetic costs explain sexual dimorphism in the circadian rhythm modulation of the electrocommunication signal of the gymnotiform fish *Brachyhypopomus pinnicaudatus*. *Journal of Experimental Biology* 211, 1012-1020.

Scheich, H., 1977. Neural basis of communication in the high frequency electric fish, Eigenmannia virescens (jamming avoidance response). *Journal of comparative physiology*, *113*(2), pp.181-206.

Sinnett, P.M., Markham, M.R. 2015. Food deprivation reduces and leptin increases the amplitude of an active sensory and communication signal in a weakly electric fish. *Hormones and Behavior* 71, 31-40.

Stoddard, P.K., 2009. Electric Signals & Electric Fish. *Dostupné z http://www2. fiu. edu/~ efish/publications/Stoddard_Electric_Signals_2009. pdf*.

Stoddard, P.K., Markham, M.R. 2008. Signal cloaking by electric fish. *BioScience* 58, 415-425.

Stoddard, P.K., Zakon, H.H., Markham, M.R. and McAnelly, L., 2006. Regulation and modulation of electric waveforms in gymnotiform electric fish. *Journal of Comparative Physiology A*, *192*(6), pp.613-624.

Stoddard, P.K., Salazar, V.L. 2011. Energetic cost of communication. *Journal of Experimental Biology* 214, 200-205.

Tinbergen, N., Perdeck, A.C. 1950. On the stimulus situation releasing the begging response in the newly hatched herring gull chick (*Larus argentatus* Pont.). *Behaviour*, 3, 1–39.

Zakon, H., Oestreich, J., Tallarovic, S. and Triefenbach, F., 2002. EOD modulations of brown ghost electric fish: JARs, chirps, rises, and dips. *Journal of Physiology-Paris*, *96*(5), pp.451-458.

Zuberbühler, K., 2001. Predator-specific alarm calls in Campbell's monkeys, Cercopithecus campbelli. *Behavioral Ecology and Sociobiology*, *50*(5), pp.414-422.

Appendices:

Figure S1: Approximated surfaces of optimal energetic strategies generated from three different column width and row height combinations (A, B, C represent reconstructed surfaces using column width = 0.25, 0.5, 1 mV and row heights = 5, 10, 20 Hz) of the grid plane that were compared and produced highly similar structures, indicating the reliability of this reconstruction method. The surface from grid width of 0.5 mV and row height of 10 Hz was arbitrarily chosen as a representation. 2.22% (721 out of 32,548) of data points in the complete data set were identified as the subset of the lower boundary that represented optimal energetic efficiency.

Figure S2: Frequency measurements of all 8 tested fish during **(A)** up-jamming experiments, **(B)** down-jamming experiments, and **(C)** white-noise experiments. Red dots represent recordings of baseline and recovery periods. Blue dots represent recordings during the stimulus period.

Figure S3: Amplitude measurements of all 8 tested fish during **(A)** up-jamming experiments, **(B)** down-jamming experiments, and **(C)** during white-noise experiments. Black dots represent recordings of baseline and recovery periods. Blue dots represent recordings during the stimulus period.

Figure S1:

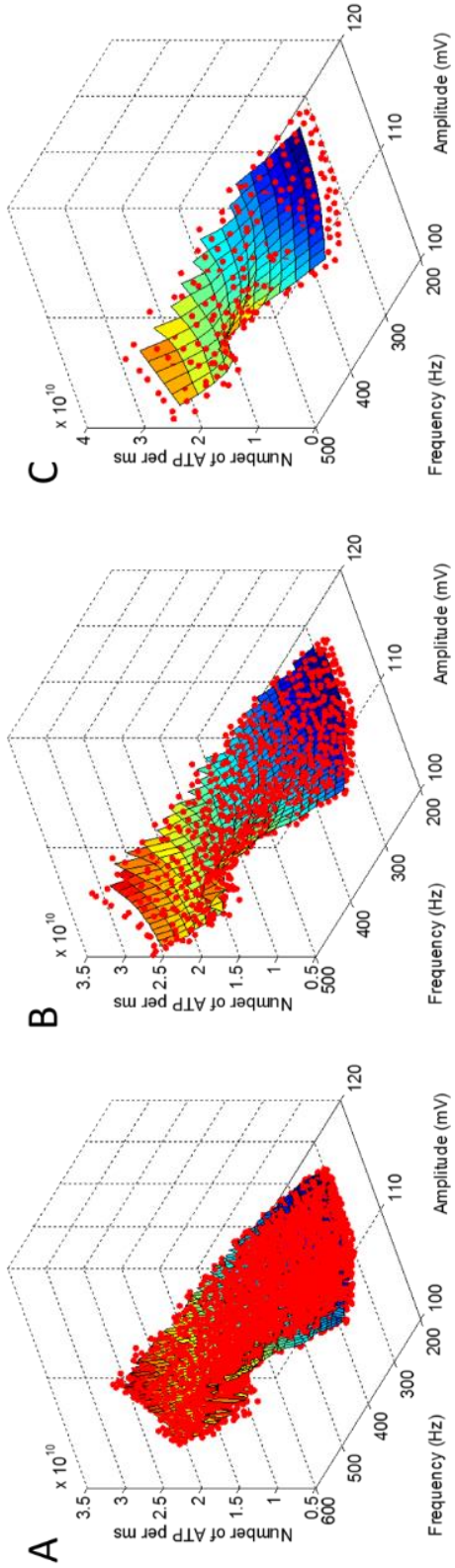

Figure S2A:

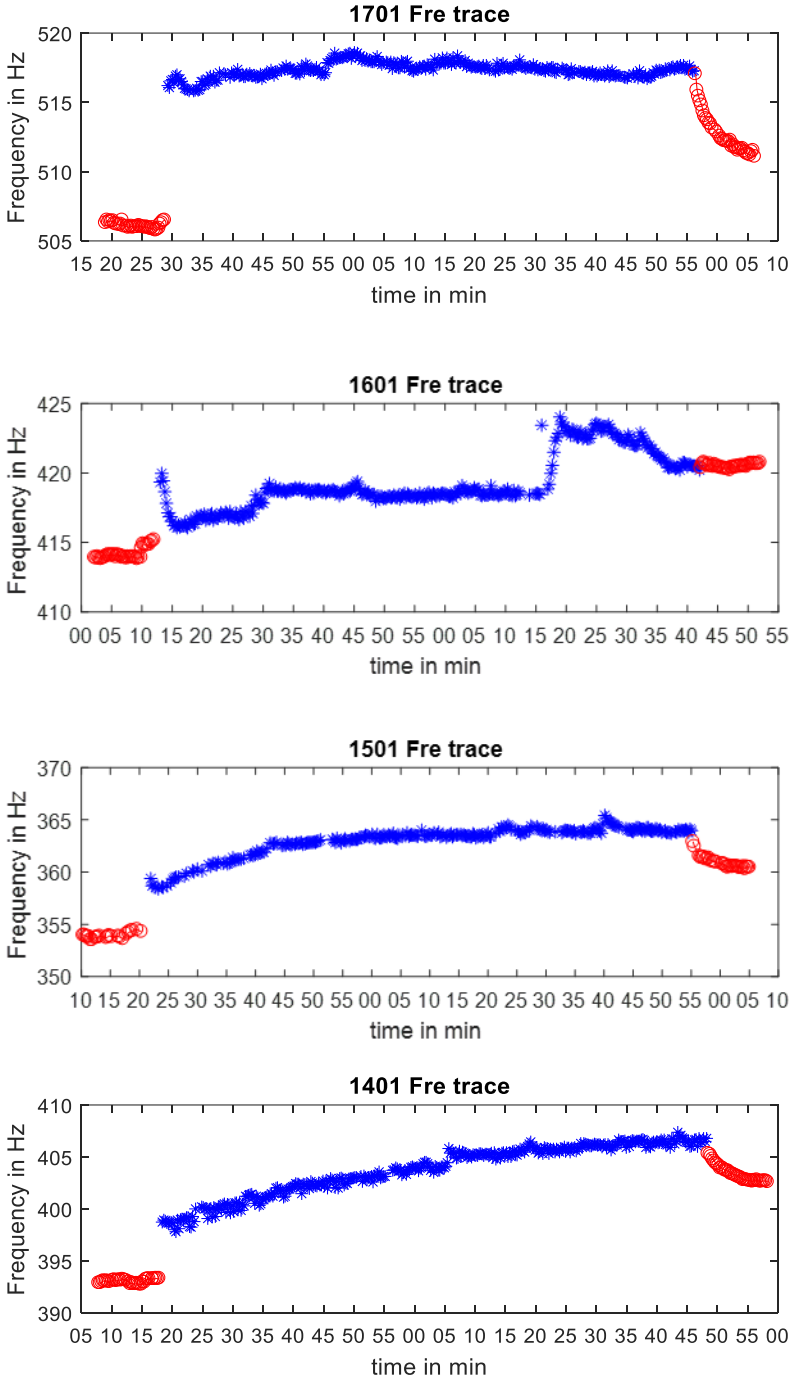
1701 Fre trace
Frequency in Hz
520
515
510
505
15 20 25 30 35 40 45 50 55 00 05 10 15 20 25 30 35 40 45 50 55 00 05 10
time in min
1601 Fre trace
Frequency in Hz
425
420
415
410
00 05 10 15 20 25 30 35 40 45 50 55 00 05 10 15 20 25 30 35 40 45 50 55
time in min
1501 Fre trace
Frequency in Hz
370
365
360
355
350
10 15 20 25 30 35 40 45 50 55 00 05 10 15 20 25 30 35 40 45 50 55 00 05 10
time in min
1401 Fre trace
Frequency in Hz
410
405
400
395
390
05 10 15 20 25 30 35 40 45 50 55 00 05 10 15 20 25 30 35 40 45 50 55 00
time in min

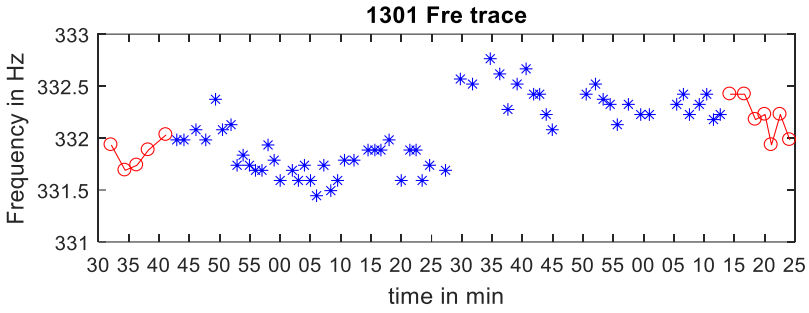
1301 Fre trace
Frequency in Hz
333
332.5
332
331.5
331
30 35 40 45 50 55 00 05 10 15 20 25 30 35 40 45 50 55 00 05 10 15 20 25
time in min

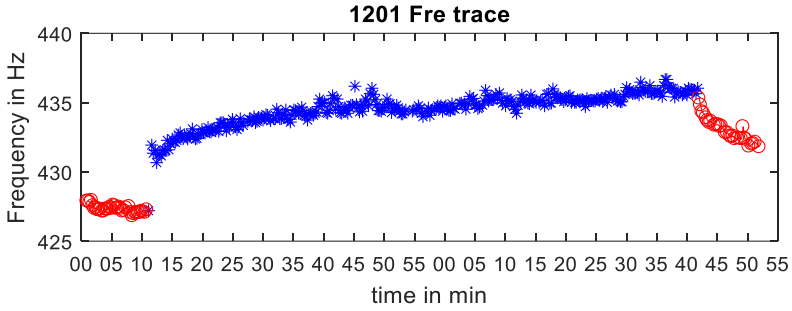
1201 Fre trace
Frequency in Hz
440
435
430
425
00 05 10 15 20 25 30 35 40 45 50 55 00 05 10 15 20 25 30 35 40 45 50 55
time in min

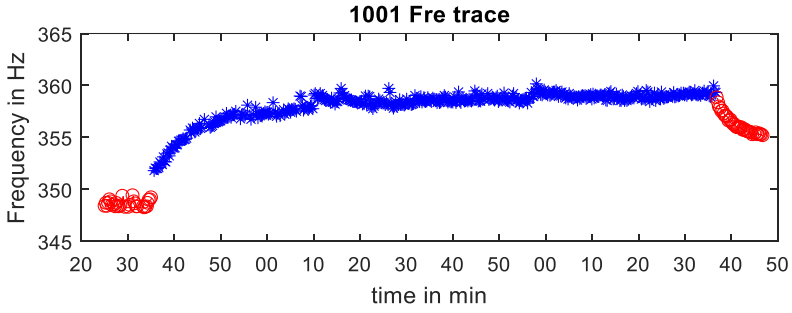
1001 Fre trace
Frequency in Hz
365
360
355
350
345
20 30 40 50 00 10 20 30 40 50 00 10 20 30 40 50
time in min

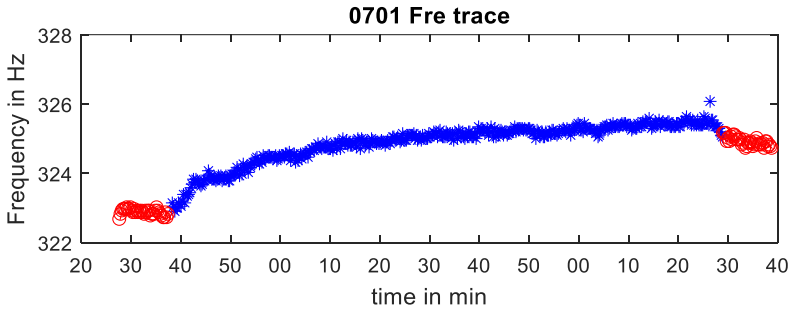
0701 Fre trace
Frequency in Hz
328
326
324
322
20 30 40 50 00 10 20 30 40 50 00 10 20 30 40
time in min

Figure S2B:

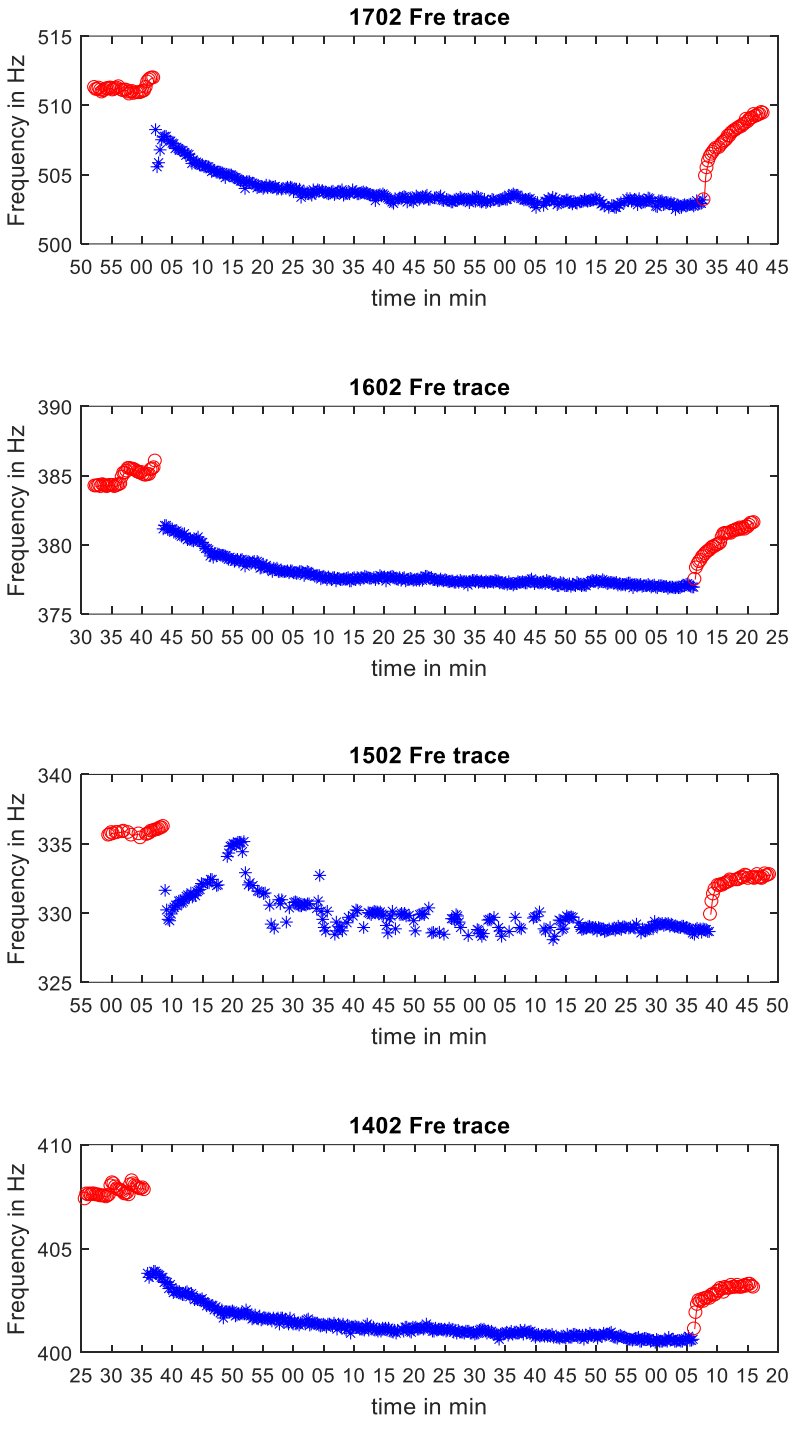
1702 Fre trace
Frequency in Hz
515
510
505
500
50 55 00 05 10 15 20 25 30 35 40 45 50 55 00 05 10 15 20 25 30 35 40 45
time in min
1602 Fre trace
Frequency in Hz
390
385
380
375
30 35 40 45 50 55 00 05 10 15 20 25 30 35 40 45 50 55 00 05 10 15 20 25
time in min
1502 Fre trace
Frequency in Hz
340
335
330
325
55 00 05 10 15 20 25 30 35 40 45 50 55 00 05 10 15 20 25 30 35 40 45 50
time in min
1402 Fre trace
Frequency in Hz
410
405
400
25 30 35 40 45 50 55 00 05 10 15 20 25 30 35 40 45 50 55 00 05 10 15 20
time in min

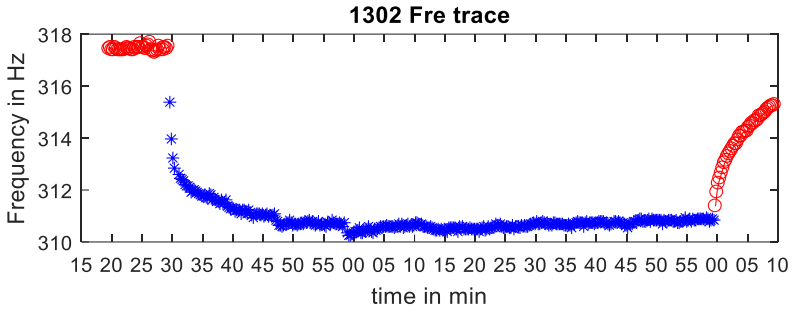
1302 Fre trace
Frequency in Hz
318
316
314
312
310
15 20 25 30 35 40 45 50 55 00 05 10 15 20 25 30 35 40 45 50 55 00 05 10
time in min

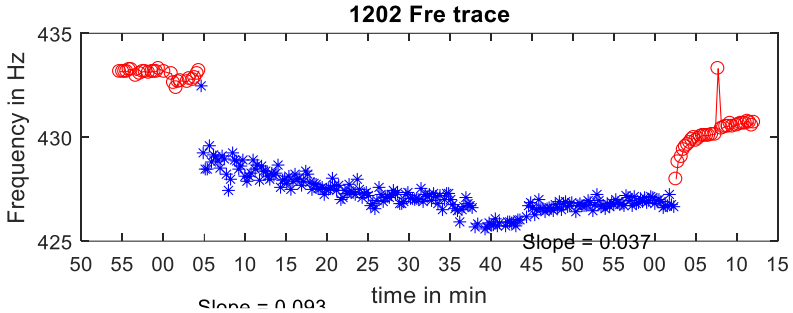
1202 Fre trace
Frequency in Hz
435
430
425
50 55 00 05 10 15 20 25 30 35 40 45 50 55 00 05 10 15
Slope = 0.037
time in min

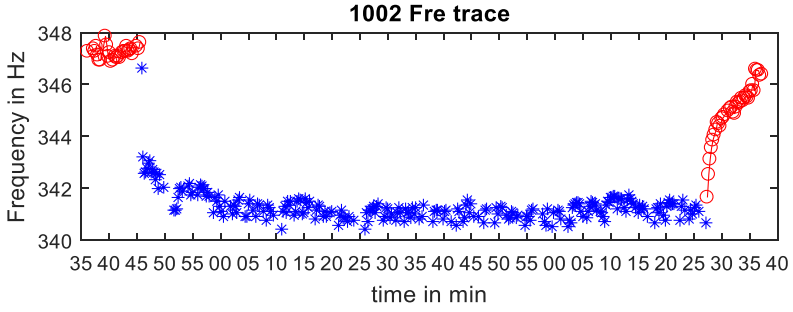
1002 Fre trace
Frequency in Hz
348
346
344
342
340
35 40 45 50 55 00 05 10 15 20 25 30 35 40 45 50 55 00 05 10 15 20 25 30 35 40
time in min

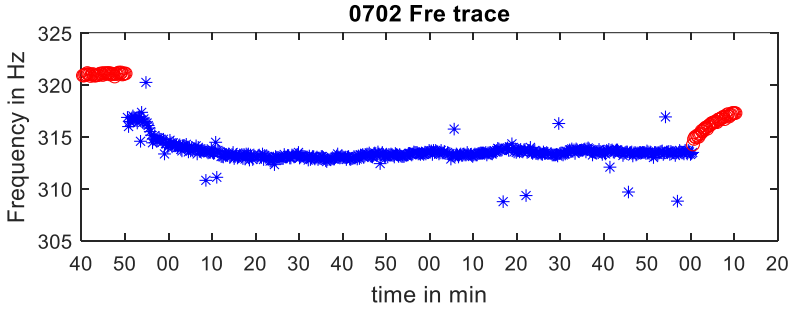
0702 Fre trace
Frequency in Hz
325
320
315
310
305
40 50 00 10 20 30 40 50 00 10 20 30 40 50 00 10 20
time in min

Figure S2C:

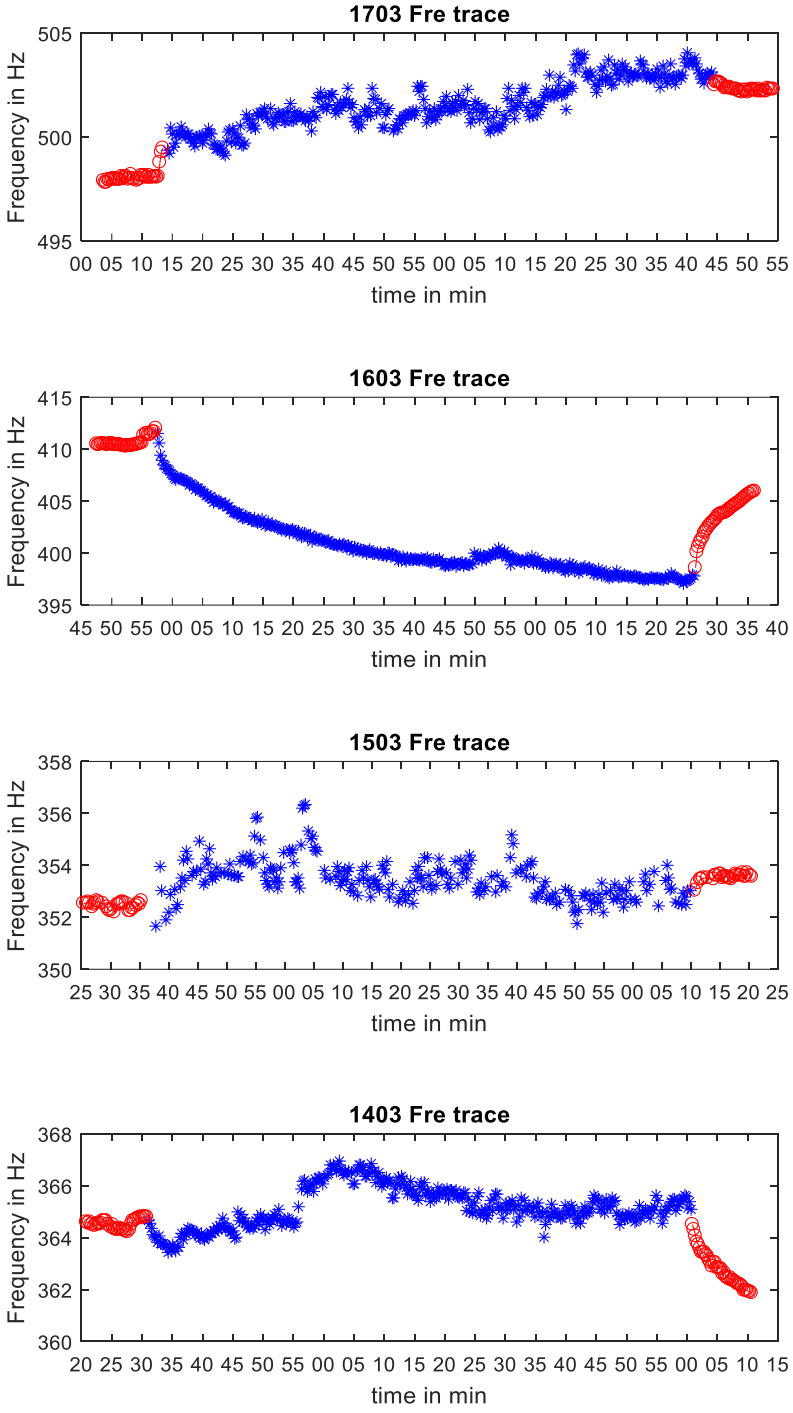
1703 Fre trace
Frequency in Hz
505
500
495
00 05 10 15 20 25 30 35 40 45 50 55 00 05 10 15 20 25 30 35 40 45 50 55
time in min
1603 Fre trace
Frequency in Hz
415
410
405
400
395
45 50 55 00 05 10 15 20 25 30 35 40 45 50 55 00 05 10 15 20 25 30 35 40
time in min
1503 Fre trace
Frequency in Hz
358
356
354
352
350
25 30 35 40 45 50 55 00 05 10 15 20 25 30 35 40 45 50 55 00 05 10 15 20 25
time in min
1403 Fre trace
Frequency in Hz
368
366
364
362
360
20 25 30 35 40 45 50 55 00 05 10 15 20 25 30 35 40 45 50 55 00 05 10 15
time in min

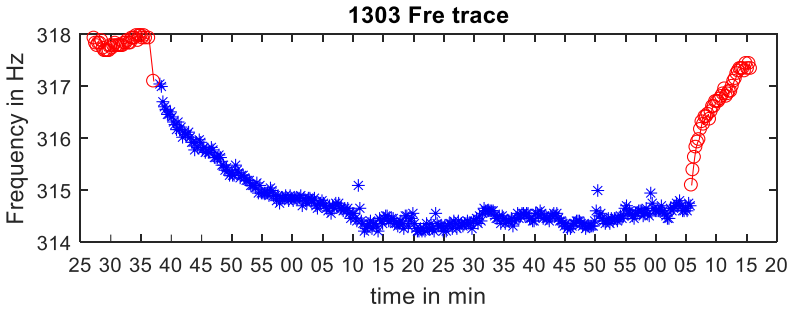
1303 Fre trace
Frequency in Hz
318
317
316
315
314
25 30 35 40 45 50 55 00 05 10 15 20 25 30 35 40 45 50 55 00 05 10 15 20
time in min

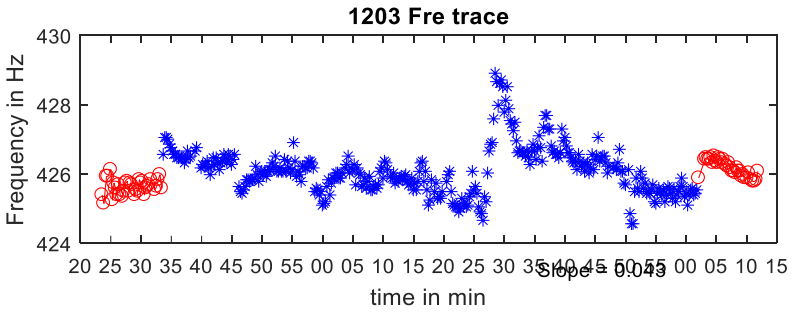
1203 Fre trace
Frequency in Hz
430
428
426
424
20 25 30 35 40 45 50 55 00 05 10 15 20 25 30 35 40 45 50 55 00 05 10 15
Slope = 0.043
time in min

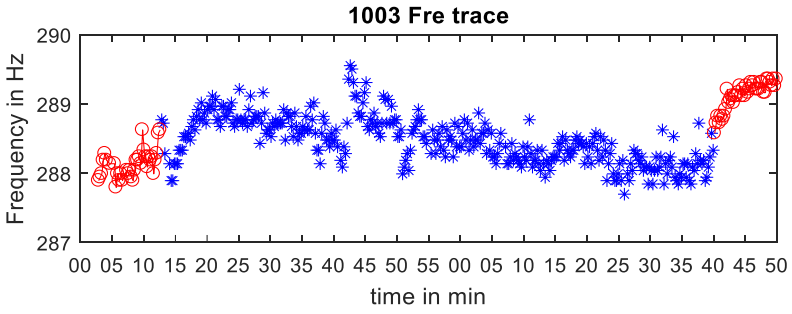
1003 Fre trace
Frequency in Hz
290
289
288
287
00 05 10 15 20 25 30 35 40 45 50 55 00 05 10 15 20 25 30 35 40 45 50
time in min

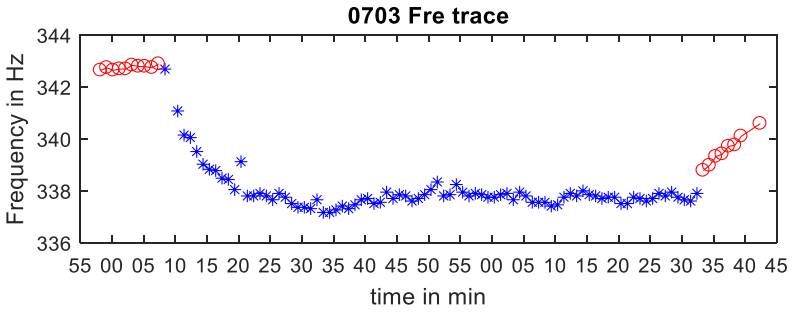
0703 Fre trace
Frequency in Hz
344
342
340
338
336
55 00 05 10 15 20 25 30 35 40 45 50 55 00 05 10 15 20 25 30 35 40 45
time in min

Figure S3A:

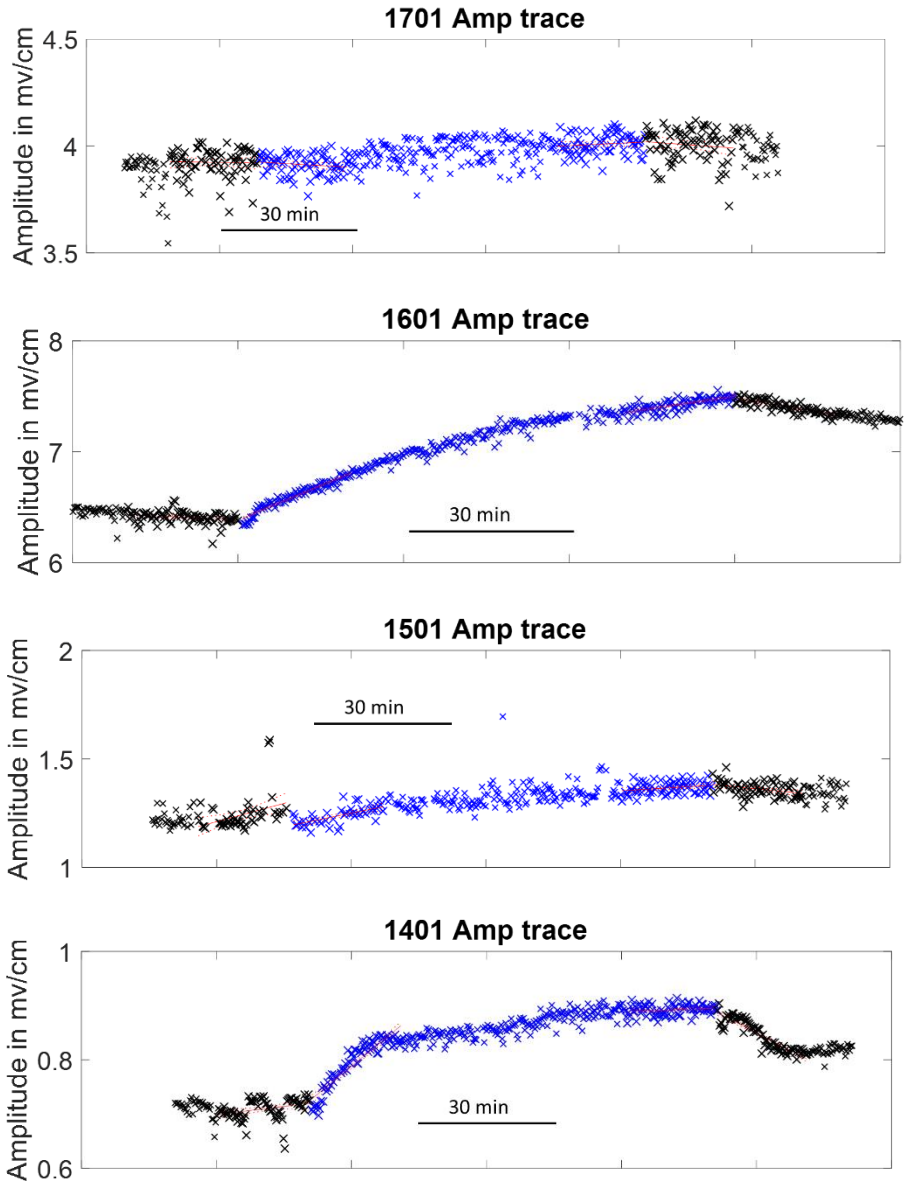
1701 Amp trace
Amplitude in mv/cm
4.5
4
3.5
30 min
1601 Amp trace
Amplitude in mv/cm
8
7
6
30 min
1501 Amp trace
Amplitude in mv/cm
2
1.5
1
30 min
1401 Amp trace
Amplitude in mv/cm
1
0.8
0.6
30 min

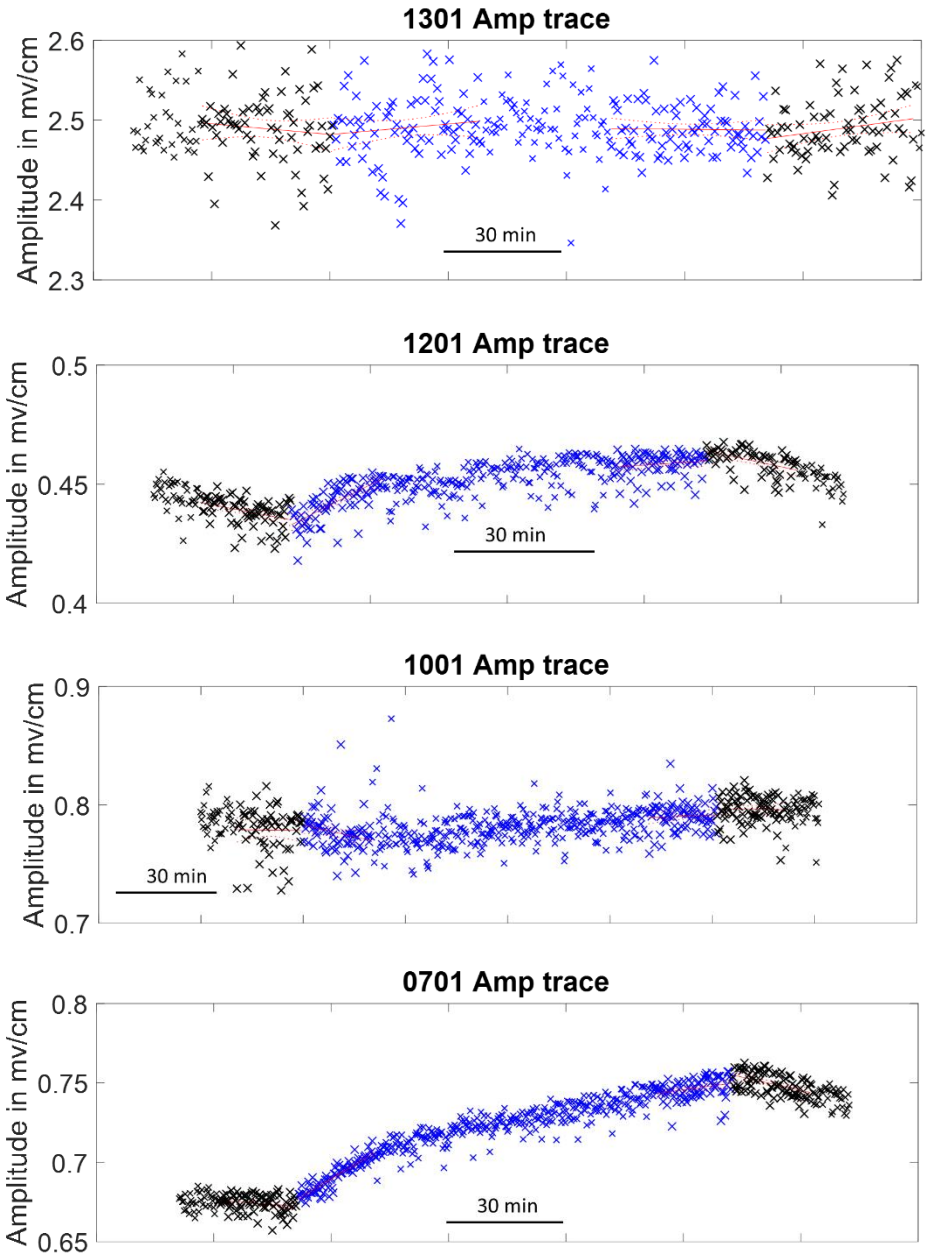
1301 Amp trace
Amplitude in mv/cm
2.6
2.5
2.4
2.3
30 min
1201 Amp trace
Amplitude in mv/cm
0.5
0.45
0.4
30 min
1001 Amp trace
Amplitude in mv/cm
0.9
0.8
0.7
30 min
0701 Amp trace
Amplitude in mv/cm
0.8
0.75
0.7
0.65
30 min

Figure S3B:

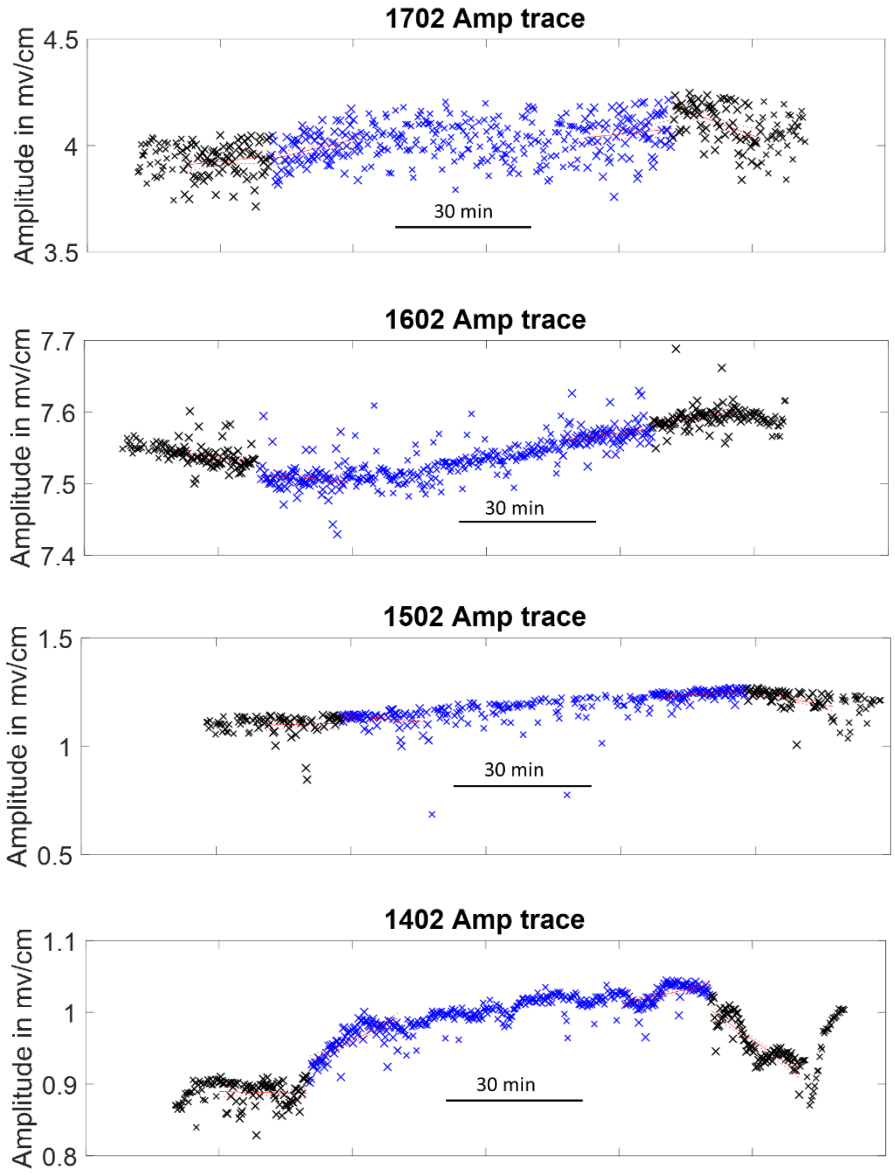
1702 Amp trace
Amplitude in mv/cm
4.5
4
3.5
30 min
1602 Amp trace
Amplitude in mv/cm
7.7
7.6
7.5
7.4
30 min
1502 Amp trace
Amplitude in mv/cm
1.5
1
0.5
30 min
1402 Amp trace
Amplitude in mv/cm
1.1
1
0.9
0.8
30 min

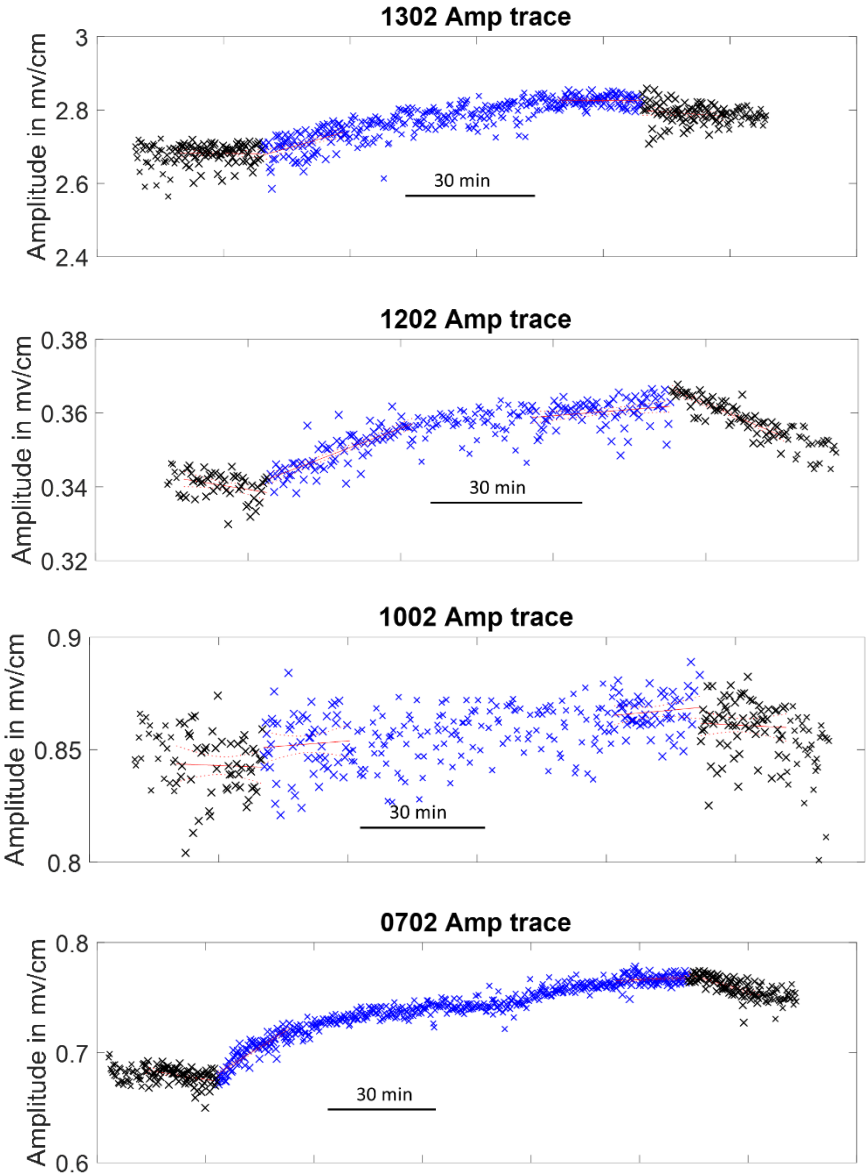
1302 Amp trace
Amplitude in mv/cm
3
2.8
2.6
2.4
30 min
1202 Amp trace
Amplitude in mv/cm
0.38
0.36
0.34
0.32
30 min
1002 Amp trace
Amplitude in mv/cm
0.9
0.85
0.8
30 min
0702 Amp trace
Amplitude in mv/cm
0.8
0.7
0.6
30 min

Figure S3C:

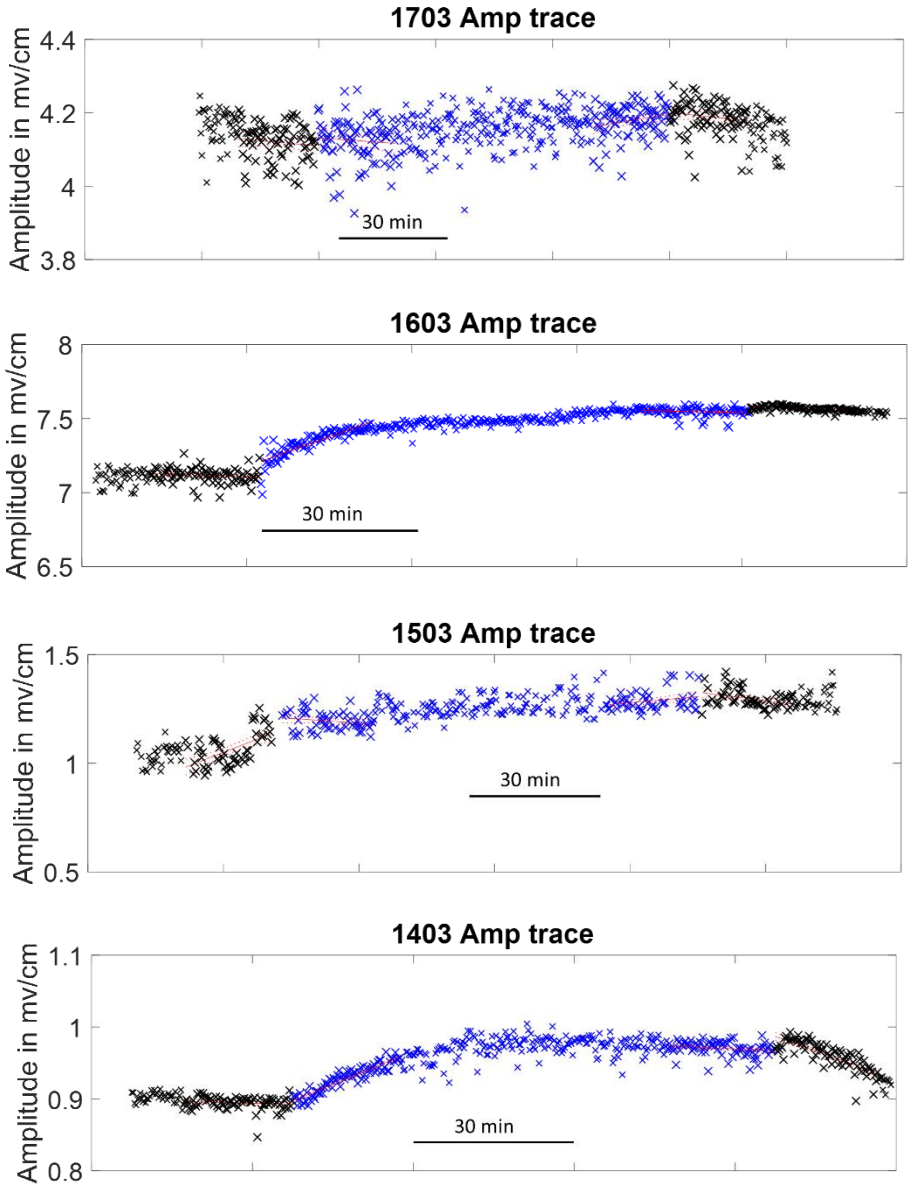
1703 Amp trace
Amplitude in mv/cm
4.4
4.2
4
3.8
30 min
1603 Amp trace
Amplitude in mv/cm
8
7.5
7
6.5
30 min
1503 Amp trace
Amplitude in mv/cm
1.5
1
0.5
30 min
1403 Amp trace
Amplitude in mv/cm
1.1
1
0.9
0.8
30 min

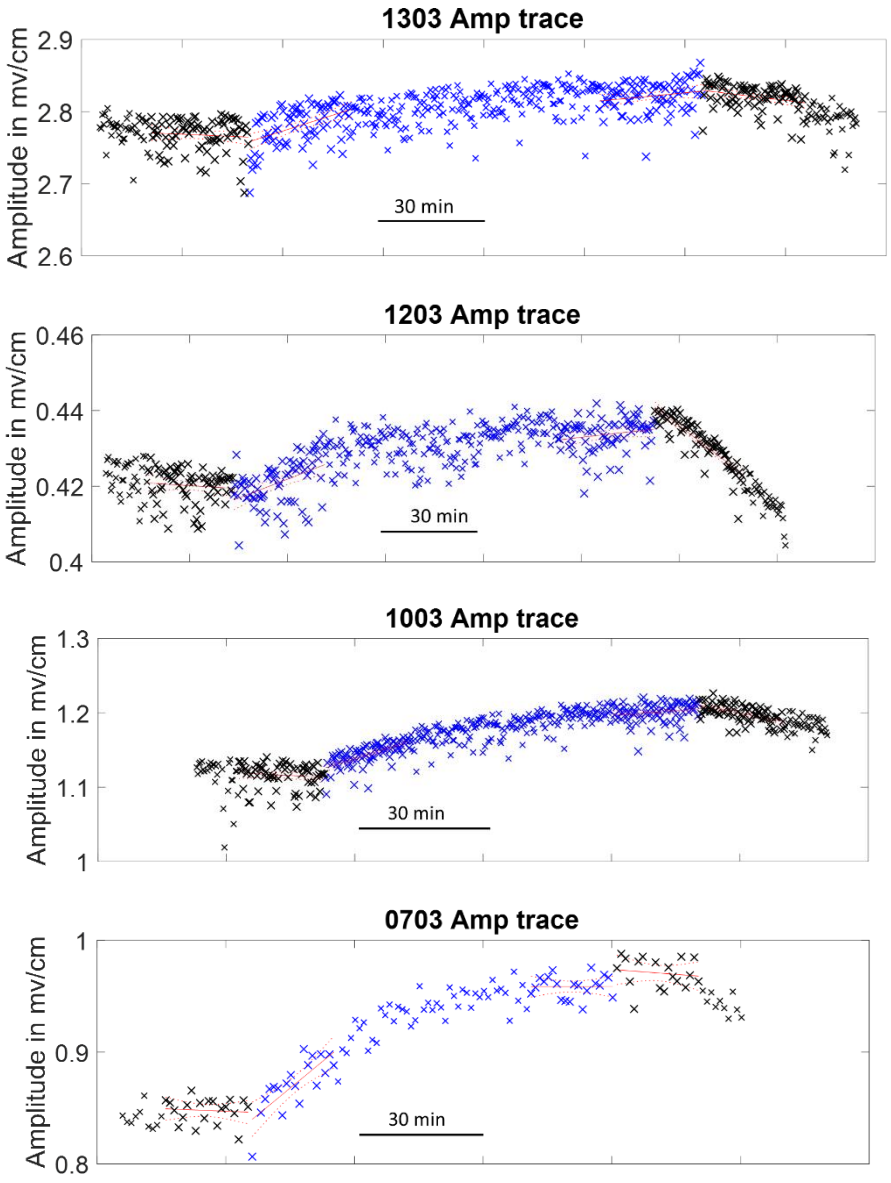
1303 Amp trace
Amplitude in mv/cm
2.9
2.8
2.7
2.6
30 min
1203 Amp trace
Amplitude in mv/cm
0.46
0.44
0.42
0.4
30 min
1003 Amp trace
Amplitude in mv/cm
1.3
1.2
1.1
1
30 min
0703 Amp trace
Amplitude in mv/cm
1
0.9
0.8
30 min